Master of Engineering

Study of Enhanced Synergistic Effect of Homobifunctional Imidoester Modified ZnO for Antibiotics

The graduate School

of the University of Ulsan

Department of Medical Science

Qingshuang Zou

Study of Enhanced Synergistic Effect of Homobifunctional Imidoester Modified ZnO for Antibiotics

Supervisor: Sung-Han, Kim

A Dissertation

Submitted to

The Graduate School of the University of Ulsan

in partial Fulfillment of the Requirements for The Degree of

Master of Engineering

by

Qingshuang Zou

Department of Medical Science

Ulsan, Korea

August, 2021

Study of Enhanced Synergistic Effect of

Homobifunctional Imidoester Modified ZnO for Antibiotics

This certifies that the dissertation

of Qingshuang Zou is approved.

Committee chair Dr. Kim, Jun Ki

Committee member Dr. Kim, Sung-Han

Committee member Dr. Shin, Yong

Department of Medical Science

University of Ulsan, Korea

August, 2021

ACKNOWLEDGEMENT

After completing this thesis, I sincerely express my gratitude to all those who wrote the thesis during Ulsan University and helped me in the past two and a half years.

First of all, I would like to express my deepest gratitude to my thesis consultant, Professor Shin, for his guidance and continuous encouragement. He provided me with valuable suggestions in academic research. During the writing of this article, he spent a lot of time reading each draft and provided me with enlightening suggestions. Without his inspiration and consistent guidance, this paper cannot reach its current form.

At the same time, I would also like to thank the professors and colleagues in our school and laboratory, who have provided me with a lot of guidance and help in the past two years. Especially Fang and Qiao, they are both my friends and mentors. Meanwhile, I also need to thank the other members of the laboratory: Dr. Jang, B. Koo, Dao, Hyo Joo and Myoung gyu. They are very friendly and also given me a lot of help in my research. I will always cherish our friendship and cherish this memory. Thank you for everything you have done for me.

Finally, I am well aware that my master's research project is not very good. I also have some regrets about it. But I am sure that as a learner, I must have the confidence to go on and will get better and better in the future.

Thank you for your help. Author Qingshuang Zou

ABSTRACT

Resistance to antibiotics due to abuse and abuse is one of the world's biggest public health challenges. Although advanced nanotechnology is used in the production of antibiotics, due to side effects such as blood clotting, toxicity, low efficacy and low biocompatibility, new types of nanomaterial composite materials are needed to cope with these effects. We first introduce a simple method that can synthesize Homobifunctional Imidoester-coated nano-spindle (HINS) zinc oxide composites with the same biological functions to enhance the efficacy of antibiotics and reduce toxicity and coagulation. The antibiotic efficacy of the composite material is twice that of commercial zinc nanoparticles. In addition, due to the covalent acylation group of HI, they have good biocompatibility, increased surface charge and solubility, and produce a large amount of Zn^{2+} ions and defensive reactive oxygen species (ROS), which can effectively kill bacteria and fungi. *In vitro* and *in vivo* experiments, in the low-dose and low-dose treatment of intravenous administration, the synergistic effect of the combination therapy of HINS complex and itraconazole showed that the destruction rate of fungi exceeded 90%. Therefore, in the medical field, HINS composite materials can be used to reduce the abuse and the impact of antibiotic abuse.

Next, BP(black phosphorus) is used as a new type of two-dimensional nanomaterials with good photothermal and drug loading properties in medical anti-tumor and biosensor research. For the first time, we tried to use the photothermal properties of black phosphorous to conduct research on disease diagnosis and other aspects, with the goal of providing more convenient and fast diagnostic techniques. Here, we use the BP and laser to irradiate the

temperature to make the *E. coli* cleavage and split the DNA, and then use HI to bind the BP and DNA, which is more conducive to the enrichment of DNA. Compared with the commercialized QIAGEN kit and Observed by Real-time PCR technology, the extraction efficiency of DNA will be more significantly improved. This provides new ideas for the future direction of black phosphorus in the molecular diagnosis of pathogens and lays a good foundation.

Keywords: Nanomaterials, Homobifunctional Imidoesters, Antibacterial, DNA extraction

CONTENTS

LIST OF FIGURES

LIST OF ABBREVIATION

BP	Black Phosphorus
BP-NIR-HI	Black Phosphorus-NIR Laser- Homobifunctional Imidoester
CTAB	Cetyltrimethylammonium Bromide
DMP	Dimethyl Pimelimidate
DMS	Dimethyl Suberimidate
DNA	Deoxyribonucleic Acid
DW	Distilled Water
FE-SEM	Field-Emission Scanning Electron Microscopy
FTIR	Flight Test Instrumentation Requirements
HI	Homobifunctional Imidoester cross-linkers
HINS	Homobifunctional Imidoester ZnO Oxide Nanoparticles
min(s)	Minute(s)
Nano-ZnO	ZnO Nanoparticles
NS-ZnO	Nano Spondle ZnO Oxide
PCR	Polymerase Chain Reaction
Real time PCR	Real-time quantitative Polymerase Chain Reaction
RT	Room Temperature
ROS	Reactive Oxygen Species
ZnO	Zinc Oxide
ZnO NPs	ZnO Oxide Nanoparticles

INTRODUCTION

At present, the incidence of microbial infections and serious side effects in the world's health facilities is increasing [1-3]. Bacterial resistance is so widespread and deadly dangerous that it has become a worldwide problem, bringing treatment difficulties to doctors from all regions. According to a 2014 study by Gould and Bal [3-6], these antibiotic-resistant bacteria can be transmitted to humans or animals. Some common antibiotic-resistant pathogens are methicillin-resistant Staphylococcus aureus (MRSA), overtoxin-producing Clostridium difficile, broad-spectrum b-lactam, and carbapenemase Coliform bacteria. The general public's ignorance of such an important issue, and the lack of alternatives to antibiotic treatment has turned it into a global crisis. Therefore, there is an urgent need to discover new antibacterial drugs to fight drug-resistant pathogens and reduce the mortality of diseases related to drug resistance, which will help limit the problem of microbial resistance on a global scale. At present, the research directions of antibacterial mainly include microbial antibiotics (nisin), plant extracts (essential oils) and nanomaterials (silver nano). However, the preparation cost of microbial antibacterial agents is relatively high, and the stability of plant extracts is not good. These two new antibacterial agents have certain limitations in practical applications. Therefore, nanomaterials have easy synthesis, good biocompatibility, and the ability to exert antibacterial activity by acting on multiple microbial targets simultaneously. Nanomaterials have become an ideal substitute for traditional antibacterial agents [7-9].

Among many nanomaterials, zinc oxide (ZnO) belongs to II-VI transition metal oxide. It

is the oxide physicochemical and photoelectric properties that have been widely studied for interesting reasons. Therefore, it is used in many fields in the field of catalysis. Sensors, medicines, personal care products, paints, batteries, solar cells, storage devices, electronics and spintronics, as well as in different documents mentioned that ZnO is used in agriculture to control crop diseases and as biological fertilizers. field. Especially due to its chemical stability, biocompatibility, and biodegradability, it has been widely used as an antifouling agent for antifouling applications and radiation protection-helping to degrade organic pollutants in wastewater treatment, etc. [10]. Zinc oxide, an ideal inorganic antibacterial agent, has broad application prospects in inhibiting food-borne spoilage and anti-pathogenic fungi [11-12].

With the continuous deepening of research on nanoparticles, nano-ZnO can be prepared by solid-phase, liquid-phase, gas-phase and other methods, among which commercial nano-ZnO is mainly prepared by liquid-phase method and gas-phase method. Phase method [13-14]. The liquid phase method has unparalleled advantages in the preparation of nanomaterials. Its characteristics are low production cost, low equipment requirements, simple operation, and easy control of reaction conditions. The commonly used liquid phase methods for preparing nano-zinc oxide mainly include precipitation method, sol-gel method, microemulsion method, hydrothermal method, etc [15-16]. Due to the influence of factors such as preparation methods, reaction conditions, substrate selection, etc., nano-effects such as steric hindrance, polar functional group guidance, charged group interactions and nanoparticle self-assembly can be triggered. So, in the case of surface polarization charges and surface broken bond atoms. Zinc oxide can form nanostructures with different

morphologies and sizes [17]. At present, the preparation of zinc oxide nanomaterials has made great progress, but there is still a big gap with industrial-scale production. In order to realize simple, convenient, environmentally friendly and low-cost industrial production technology of Nano-zinc oxide materials, it is still necessary to explore [18]. Therefore, the simplified synthesis method used herein is used to obtain spindle-shaped zinc oxide. Compared with the traditional laboratory method of synthesizing zinc oxide, the synthesized zinc oxide has the advantages of time saving, stable performance and uniform particle size.

Nano-ZnO has received widespread attention due to its excellent antibacterial properties, but there are still some problems in the antibacterial research of Nano-ZnO [19-20]. First, the antibacterial properties of Nano-ZnO are mainly focused on bacteria. Compared with bacteria, fungi have more complex tissue structures and physiological regulation systems, so the antibacterial properties of nanomaterials cannot fully represent their antifungal properties [21-22]. Secondly, the types and properties of nanomaterials vary greatly, and the stress effects of different nanomaterials on microorganisms are not completely consistent. There is no unified conclusion on the mechanism of nanomaterials on fungi [23-24]. In addition, studies on the biocompatibility of zinc oxide have different toxicity in different animal cells [25].

Therefore, here I report a new method for synthesizing spindle-shaped nano-zinc oxide, which can be modified by HI (DMS or DMP) to obtain composite materials that can significantly enhance antibacterial and antifungal properties [26-28]. which is the continuous accumulation of CTAB and $Zn(NO_3)_2 \cdot 6H_2O$ in an alkaline environment to become a spindle-shaped ZnO with a diameter of 200nm (NS-ZnO). Compared with the traditional

synthesis method, the synthesis time and operation steps of the material are obviously shortened. Then it is modified by surfactant HI (DMS or DMP). The purpose is to increase the positive charge on the surface of the material and obtain a large amount of dendritic HI structure on the materials' surface, which is more conducive to improving the stability of the material, and the material will be easier to integrate the pathogenic bacteria bind tightly [29-30]. Objective to obtain a composite material that can significantly enhance antibacterial and antifungal properties. In addition, according to the specificity of its physical form (Shuttle-like and spindle-shaped), the increase of surface positive charge, the production of Zn^{2+} and the mass production of ROS during the release process, the sterilization mechanism of the composite material is explained. And through the antifungal test in combination with antifungal drugs, it is proved that the combination therapy has a good synergistic antifungal effect. Finally, in vivo animal experiments in mice show that the composite material has no obvious toxic side effects on the blood and organs of mice. At the same time, it also proved that the new ZnO composite nanomaterial has good biocompatibility. And it has laid the foundation for its future clinical antibacterial treatment.

In another biological application related to nanomaterials, black phosphorus was selected as the research object. Black phosphorus, as a representative of two-dimensional materials [31-33]. It has excellent biocompatibility, photothermal properties and drug loading. In recent years, the application in biology has become more and more extensive [34-36]. Here, I tried for the first time by using black phosphorous nanosheets to be sonicated and broken into black phosphorous nanoparticles (50~100nm) with good dispersibility, and by using black phosphorous and *E.coli* samples after being irradiated with 808nm laser , Allowing

bacterial cells to lyse and release DNA. Then, the black phosphorus is bound to DNA by HI (DMS), and the complex of black phosphorus and DNA is precipitated by centrifugation. Under the action of HI, a large amount of DNA can be enriched in the precipitate. Finally, after alkaline Elution buffer (pH 10.6), the HI connection between black phosphorus and DNA is broken, and a large amount of DNA can be dispersed in Elution buffer, and then centrifuged to obtain a high-concentration DNA supernatant solution. Here, I named this method of extracting DNA using black phosphorescence thermally as the BP-NIR-HI system. Contrast with the traditional commercial QIAGEN DNA extraction kit. The BP-NIR-HI system method of extracting DNA in the same concentration of *E. coli* samples can first obtain a higher content of black phosphorus. Secondly, compared with the QIAZEN kit, it is different from using enzymes to dissolve DNA, which will cause DNA damage to a certain extent. The photothermal method extracts DNA to obtain complete DNA. At the same time, compared with the kit to extract DNA, BP-NIR-HI can use less time and fewer experimental steps to obtain DNA, thereby improving the efficiency of DNA extraction in biological applications. Therefore, black phosphorus has great potential in biological diagnosis and detection, laying a foundation for the future application of this two-dimensional nanomaterial in the field of biomedicine.

1. MATERIALS AND METHODS

2.1. Chemicals and reagents

All experimental reagents were analytically pure and used without further purification. Zinc nitrate hexahydrate ($ZnNO_3 \bullet 6H_2O$, 98%), ammonium hydroxide solution (28% NH_3 in H_2O, 99.99% trace metal reference), dimethyl pimelimidate dihydrochloride (DMP, Sigma, D8388-5G), dimethyl suberimidate dihydrochloride (DMS, Sigma, 179523-5G), 2',7'-dichlorofluorescein (batch # BCBZ6854), Itraconazole (catalog number I6657-100MG) and 2',7'-dichlorofluorescein (DCF) (catalog number BCBZ6854) were purchased from Sigma-Aldrich (St. Louis, Missouri, USA). Cetyltrimethylammonium bromide ($C_{19}H_{42}BrN$, > 98%, CTAB) was purchased from the Tokyo Chemical Industry Co. Ltd. (Tokyo, Japan). Dulbecco's modified eagle medium (DMEM; Life Technologies, Carlsbad, California, USA). 3-(4,5-Dimethylthiazol-2-yl)-2,5-Diphenyltetrazolium Bromide (MTT kit, lot number.M6494, ThermoFisher). LB medium was used for bacterial culture; Sabot's dextrose agar and chloramphenicol medium containing chloramphenicol medium (catalog number: C6781; lot number: 437412) were purchased from Santa Maria. The commercial QIAGEN amp DNA Mini Kit (DNA Mini Kit: Cat No. 51304, RNA Mini Kit: Cat No.74104. Milli-Q water and phosphate buffered saline (PBS, 10x, pH 7.4) were used in all the experiments.

2.2. Biological samples

Prokaryotic *Escherichia coli* (ATCC25922) and *Salmonella* (ATCC14028) were inoculated into the nutrient broth or LB medium and kept overnight in a shaking incubator at 37°C and 210 rpm. *Aspergillus* fungus (ATCC36607) was grown in Sabouraud dextrose agar at 25°C for 5 days. After culture, the Aspergillus fungi was re-suspended in PBS and quantified using a hemocytometer.

2.3. Preparation of the NS-ZnO and HINS composite

a) The NS-ZnO crystals were synthesized by the hydrothermal method in an alkaline medium.1 mL of 1 M $Zn(NO_3)_2 \cdot 6H_2O$ (Sigma, 228737-100G) and 1 mL of 1M cetyltrimethylammonium bromide (CTAB, DaeJung Chemicals, 2544-4105) were added to 98 mL of Milli-Q water in a 250 mL flask. The system was magnetically stirred (500 rpm) along with heating at 95 °C for 50 min. Subsequently, under steady stirring conditions, 2 mL of ammonium hydroxide solution (DaeJung Chemicals, 1065-3300) was added drop-wise to the reaction mixture. After stirring, a milky colloidal solution appeared. To stop the growth of NS-ZnO, the reaction flask was placed in a 0 °C freezer immediately. After nearly 10 min, we transferred the product into a 50 mL tube and centrifuged the solution. The supernatant liquid was removed, and the precipitate re-suspended in the Milli-Q water to wash out the residual ions. This process was repeated 3 times and finally the precipitate was dried overnight in a drying oven (Yamato, DX312C) at 56 °C.

b) To enhance the stability and biocompatibility of NS-ZnO, a homobifunctional imidoester (HI) modification was carried out. Two types of HI (DMP and DMS) were used in the tests. Briefly, 4 mg NS-ZnO (40 mg/mL, 100 μL) and 4 mg HI (DMP or DMS, 10 mg/mL, 400 μL) were dissolved in a 1.5 mL EP tube in a 500 μL solution. The mixture was oscillated by an oscillating machine (Magic-mixer TMM-5). After 12 h, the mixture was centrifuged at 12,000 rpm for 5 min (Mini-Centrifuge, Labogene). The supernatant liquid was removed, and the precipitate was washed twice by Milli-Q water. Finally, 400 μL of Milli-Q water was used to re-suspend the precipitate to obtain 10 mg/mL of HINS composite solution. The precipitate was dried overnight in a drying oven (Yamato, DX312C) at 56 °C.

2.4. Characterization

A field emission scanning electron microscope (FE-SEM) and JSM-7500F (JEOL) were used to characterize the morphology of the ZnO nanomaterials (commercial or synthetic), Black phosphorus and modified composite samples to determine the surface morphology and characteristics of the materials. Fourier transform infrared spectroscopy (FTIR) analysis of samples using JASCO 6300 (JASCO) was carried out to obtain information on the chemical modification of the materials. Energy dispersive X-ray (EDX) analysis was used to analyze the elemental composition in the composite material and a UV/visible spectrophotometer was used to determine the composite materials.

2.5. ROS detection

The commercial DCFDA ROS detection kit and modified DCFH-DA (2', 7'-dichlorofluorescein diacetate) method were used to measure the production of ROS in *E.coli* environments. The generation of basic ROS was detected by recording the fluorescence (Ex/Em: 485/535 nm) with a microplate reader. Each experiment was repeated on three different occasions (n=3). The relative fluorescence units (RFU) were calculated from all the measured values.

2.6. Antibacterials

Escherichia coli and *Salmonella* were used as the antibacterial research objects. The antibacterial activity of different types of zinc oxide and its composite materials was evaluated by using different concentrations of *E. coli* and *Salmonella* cultures as suspensions. Prior to the evaluation, the bacteria were cultured aerobically in LB medium at 37°C and a 210 rpm shaking incubator for 12 h. The bacterial cells were obtained by centrifugation at 2000 rpm for 5 min and re-suspended in LB. The bacterial suspension was diluted appropriately (to 10^4~10^5) and an aliquot of 100 μL was transferred to the agar plate. A plastic rod was used to evenly distribute the bacteria on the surface of the agar plate. After 16 hours of incubation, the colonies were counted and the colony forming units per mL (CFU/mL) of the original bacterial sample were calculated. The concentration of the bacterial suspension was adjusted to 1×10^7 CFU/mL. Equal volumes of the different nanomaterials to be tested were put into a tube containing 0.1 mL of 1×10^7 CFU/mL bacterial suspension and

2 mL of LB medium and mixed. After 12 h of incubation with shaking at 210 rpm at 37°C, we measured the absorbance of each sample at OD 600 nm (optical density，The absorbance of a substance at a particular wavelength). The bacterial survival rate of each sample was calculated and the growth curve of bacteria with respect to the nanomaterials over time was prepared by using the following formula:

$$\text{Bacteria Survival Rate}(\%) = \frac{(OD_{ZnO} - OD_{Negative})}{(OD_{Positive} - OD_{Negative})} \times 100\%$$

2.7. Antifungal Assay via Radial Growth

We used *Aspergillus* as the research object to test the effect of nanomaterials on fungi. At first, we had to prepare the fungal glucose agar medium for the antifungal test. The two methods that were used to demonstrate the influence of the tested nanomaterials on the growth of fungi are described below: (a) Many blank glucose agar medium plates to be cultured were prepared. Fungal spores were collected from 15-day old *Aspergillus* parents to obtain uniformity and reproducibility in the experiment, and we obtained 2000 spores for every 50 μL of solution. The spore solution and different concentrations of nanomaterials to be tested were thoroughly mixed and uniformly coated on the blank glucose agar medium plate, dried and placed upside down. The plate was kept in the incubator at 25 °C and from the 3rd day, a photographic record of each fungus sample was taken. Image-J was used to analyze these records, measure the number and area of colony growth, and compare the growth rate of each treatment with the control sample. (b) A specific solid medium containing different amounts of measured nanomaterials was established. Before using a petri dish,

different processing methods were adopted to ensure that the tested nanomaterials were well dispersed in the culture medium. A hole of diameter 1 cm was made at the center of each solidified medium and subsequently 400 conidia of 50 μL PBS were added to the central hole of each petri dish containing the culture medium for each treatment. The dishes were moved to the incubation furnace and kept at 25 °C. From the 5th day, a photographic record of each fungus sample was taken. Image-J was used to analyze these records, measure the growth area, and compare the growth rate of each treatment with the control sample. In addition, the synergistic effect of the nanomaterials and commercial antibiotics (6.0 μg/mL Itraconazole) was also studied by mixing the nanomaterials and commercial antibiotics with *Aspergillus,* either together or separately.

$$\text{Growth Rate of ZnO Treatment}(\%) = \frac{\text{Growth of ZnO Treatment}}{\text{Growth of Control}} \times 100\%$$

The effect of ions and pH were studied by adding the extra condition into the culture medium.

2.8. *In vitro* cell test

HCT-116 cells（CL0096, Procell） and L929（CB85523573） cells were cultured in DMEM medium containing 10% FBS, and incubated at 5% CO2 and 37°C（purchased by Thermo scientific）for 48 hours, then plated in a 96-well plate, observed and counted under a microscope to ensure 15,000 cells /100 μL per well. Different groups of composite material zinc oxide were added to the orifice plates at different concentrations. After incubating at 37°C for 24 hours, the numerical values and statistical data were obtained using MTT method. The experiment was repeated three times for each group.

2.9. *In vivo* toxicity assay

Fifty ICR mice (6 weeks old, 25 males and 25 females) were purchased from Koatech, Gyeonggi-do, South Korea and randomly divided into 5 groups where each group consisted of 10 mice, 5 males and 5 females, and fed in separate cages. The mice were maintained at room temperature (22 ± 2°C) with a light/dark cycle of 12/12 hours and sufficient food and water sources were ensured. The groups were as follows: the first group (control group), the second group (LD-NS-ZnO, low dose) in which LD-NS-ZnO was injected; the third group (HD-NS-ZnO, high dose) in which HD-NS-ZnO was injected; the fourth group (LD-HINS composite, low dose) received the LD-HINS composite. The fifth group (HD-HINS composite, high dose) received the HD-HINS composite. The mice of each sex were injected with 300 μL of ZnO composite nanomaterials by tail vein injection at a dose of 0.1 mg/mL (low dose), 1 mg/mL (high dose) or Milli-Q water (control group). After the administration,

the weight of the animal was checked every day to check whether the animal showed any adverse reactions after the injection of the drug. After 14 days of feeding, the animals were euthanized using Zoletil (Virbac, South Korea), and blood samples were collected from the abdominal aorta. A biochemical measurement of blood indicators was carried out: alanine aminotransferase (ALT), aspartate aminotransferase (AST), total bilirubin (T-Bil), blood urea nitrogen (BUN), creatinine, total protein (TP), albumin, albumin/globulin (A/G) ratio, total cholesterol (TC), triglycerides (TG), glucose, and phosphorus. The biochemical analysis of the plasma samples was performed using commercially available kits according to the manufacturer's instructions. After collecting the blood sample, the body surface was observed visually (all orifices, all internal organs of the head, abdominal cavity, and thoracic cavity as well as their contents) for obvious signs of abnormality. The body and organ weights of each mouse were measured. For grouped organs, the sum of the organs was used. The organs, including the brain, heart, lung, liver, kidney, spleen, testes, and ovary, were collected and preserved in 10% phosphate buffered formalin solution for 24 h and then dehydrated to make paraffin sections. The slides were mounted after staining with hematoxylin and eosin (H&E) and observed under an optical microscope (BX51, Olympus, Tokyo, Japan) for histopathological examination. The experimental protocol and this research were approved by the Institutional Animal Care and Use Committee of the Laboratory Animal Center of the Osong Medical Innovation Foundation (KBIO-IACUC-2020-011).

2.10. DNA extraction method

2.10.1. DNA extraction by BP-NIR-HI system:

First, the 200 μL 1×10^5 *E.coli* sample to be tested is combined with 500 μg/mL 200 μL black phosphorous nanosheet solution, and the sample is irradiated with a 3A current intensity NIR laser (was purchased from SPEEDY) to increase the temperature of the system to 55 and then keep the temperature for 5 minutes.

Then, after vortex, add 50 μL 100 mg/mL HI(DMS) to the test tube and mix for 1min, then centrifuge at 13000 rpm for 1min to remove the supernatant.

Last. Add 100μL of Elution buffer pH 10.6, mix 3~5s, and centrifuge at 13000rpm for 1min to obtain the supernatant, which is the solution containing DNA.

2.10.2. DNA extraction by QIAZEN kit：

First, mix 200 μL of 1×10^5 *E. coli* sample with 200 μL QIAZEN lysis buffer, and add 2μL of Proteinase K. Then incubate at 55°C for 10 min.

Add 200 μL of 100% alcohol to the mixed solution, transfer the liquid to the filter tube, centrifuge at 8000 rpm for 1min. After discarding the liquid, add 500 μL AW1 solution to the filtered tube. Then centrifuge at 8000 rpm and discard the liquid after centrifugation for 1 min.

Finally, add 500 μL of AW2 solution to the filtered tube, centrifuge at 13000 rpm for 3min, and discard the liquid. Finally, add 100 μL of Elution to the tube. After standing for 1 min, centrifuge at 8000 rpm for 1 min. The resulting solution is the DNA-containing solution.

2.11. DNA concentration test

Use 7500 Real-time PCR systemv(was purchased by BIO-RAD). Take 5 μL of DNA samples extracted with QIAGEN kit and BP-NIR-HI system in each group, and mix with 10 μL of Master mix, we used the following primers (*E. coli-rod A-195*): forward (5′-CACCCGTGTCTATCGTACCT-3′) and reverse (5′-ATTTCGCTGCGTTCTTCATC-3′), each is 1 μL, and 3 μL of ultrapure water. The total reaction volume is 20 μL. The PCR reactions were performed at 95°C for 15 min, followed by 40 cycles of 95°C for 10 s, 60°C for 20 s, and 72°C for 20 s, before a final elongation step at 95°C for 10 s. Besides, NanoDrop 2000 spectrophotometer (PeqLab Korea) were used for the NA detection test.

3. RESULTS

CHAPTER 1 - Biomedical applications of ZnO Composite

3.1. Procedure and chemical characterization of HINS composite

The NS-ZnO(~200nm) were prepared through facile hydro-thermal method (Figure 1A), the uniform spindle-shaped NS-ZnO have been obtained with controlling the reacted-reagents ratio and stirring speed precisely. The activation energies of ZnO crystal growth at the booting of surfactant CTAB, and the special elementary layers (including compositions and thicknesses) of ZnO in hydro-thermal alkali solution resulting in the sharp sides and bulging middle structure of Nano Spindle ZnO. After HI modification, HINS can still maintain the spindle shape (HINS, SEM image in Figure 1B). The size distribution data of our studied materials were obtained by DLS detection, the size of our synthesized NS-ZnO is mainly distributed in the region of 180~200 nm (Figure. 1C).

According to the observation of the peak FTIR of the material, it is confirmed that the purity of the synthesized NS-ZnO is the same as the commercial standard. In addition, the wider shape of the HINS peaks implies the existence of special base cells forming nanometer spindles (Figure 2A). The stability of the solution was studied by measuring the zeta potential, which can quantify the potential in the interfacial layer of dispersed particles. Figure 2B shows a comparison of the initial instability of commercial ZnO NP (from -20 to -25 mV) and the intermediate stability of synthetic NS-ZnO (close to +30 mV). After being modified by HI, the surface potential of the nanomaterials all showed an increase in positive charge.

ZnO NPs-HI is close to - 10mV, HINS is close to + 40mV. As shown in the synthetic route shown in the figure, we studied dimethyl benzenemalonate (DMP) and dimethyl sulfite (DMS), as well as commercial ZnO NP and our synthesized NS-ZnO, and then studied ZnO NPs -HI and HINS composite materials. The NS-ZnO we synthesized is surrounded by NH2+, indicating that the positive zeta potential of the surface can form a covalent bond with the iminoester functional group through the amide bond (Figure 1A). To study the efficacy of HI modification, we tested a series of HI concentrations (DMS and DMP) in the complex. Studies on UV-Vis absorption spectra show that HI modified ZnO NPs have a red shift, which may be due to the energy loss caused by HI (DMP) modification and the expansion of the peak range implying the change. The particle morphology caused by melting or aggregation Change (Figure 2C). However, there is no obvious morphology of the HINS composite material to melt or gain energy (blue shift) (Figure 2D).

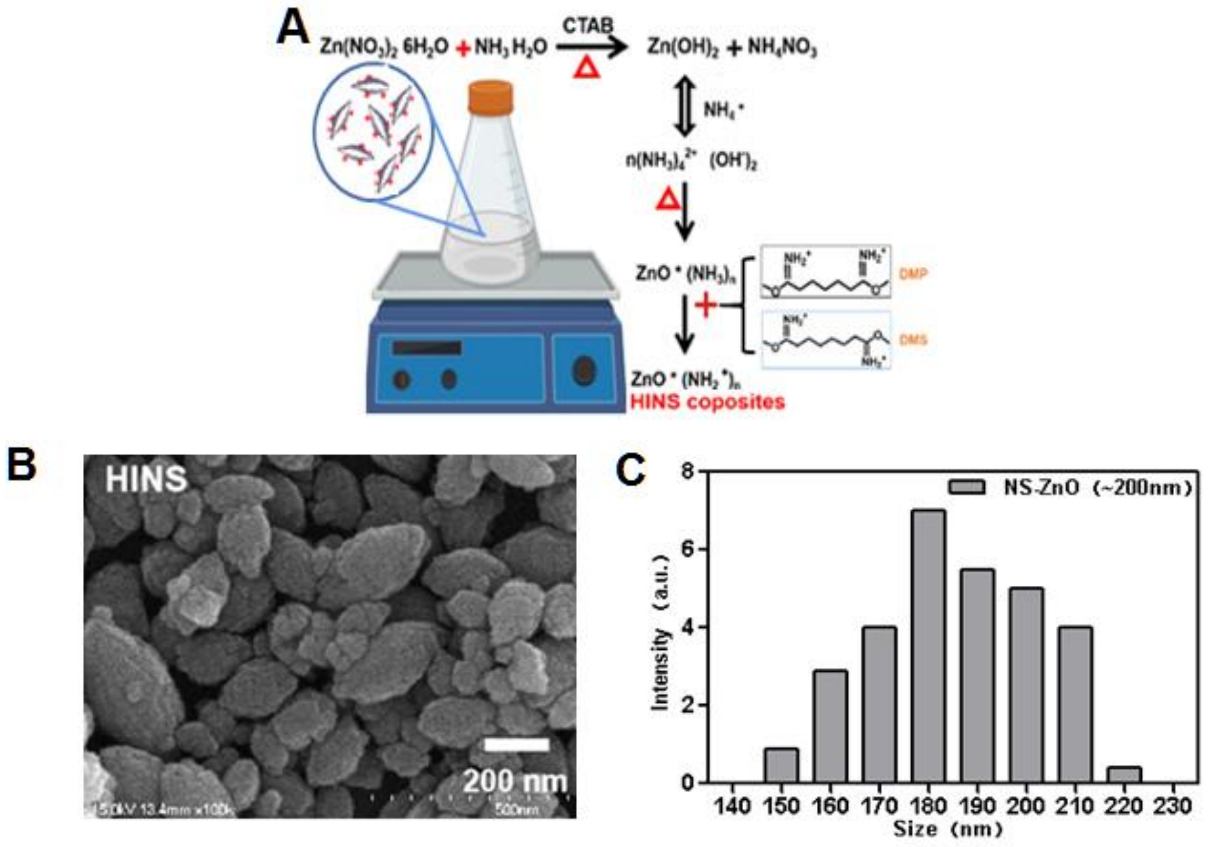

Figure1. Characterization of ZnO NPs, ZnO NPs-HI, NS-ZnO, and HINS composite. (A) Schematic of the structure and synthetic routine of HINS composite. (B) Scanning electron microscopy (SEM) images of the synthesized HINS (~200 nm) in uniform nanospindle structure. (C) Dynamic light scattering (DLS) analysis of the size distribution of synthesized NS-ZnO.

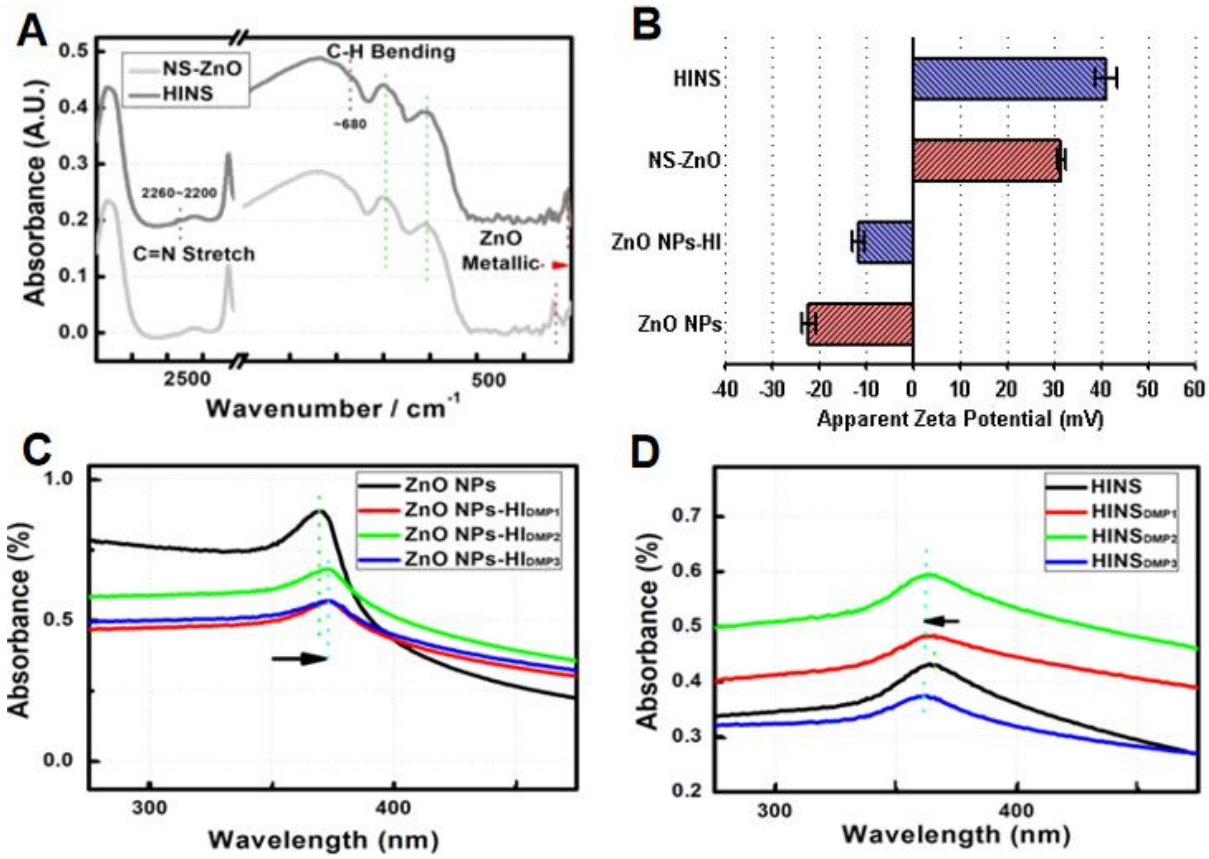

Figure 2. Characterization of ZnO NPs, ZnO NPs-HI, NS-ZnO, and HINS composite. (A) FTIR result of our ZnO nanomaterials (ZnO NPs and NS-ZnO). (B) Zeta potentials of our materials ZnO NPs (~100 nm); NS-ZnO (~200 nm); ZnO NPs-HI (~200nm) and HINS (~200nm). (C) UV–visible absorption spectra of the ZnO NPs and the material after HI(DMP) modification (ZnO NPs-HI) with a red shift. (D) UV–visible absorption spectra of the NS-ZnO and the material after HI (DMP) modification (HINS composite) with a blue shift.

3.2. Antibiotic activity of the HINS composite nanomaterial

The use of model microorganisms (Gram-negative bacteria *Escherichia coli* and *Salmonella*) proved the antibacterial efficiency of the HINS composite. The tested ZnO NPs, ZnO NPs-HI, NS-ZnO and HINS composite nanomaterials were added to the bacterial culture solution at different concentrations. After culturing for 12 hours, the viability of each group of bacteria was studied (Figure 3B). The results showed that at a concentration of 4 μg/mL, the HINS composite completely inhibited the growth of pathogens, which has a higher efficiency than other ZnO nanomaterials (NS-ZnO and ZnO NPs). At the same concentration, the antibacterial effect of NS-ZnO is better than that of ZnO NPs, which may be due to its active surface characteristics (positive surface charge is easy to attract bacteria) and physical form (the sharp sides of NS-ZnO pierce the bacteria). These inferences can be reconfirmed by observing the lysed glass slide, where NS-ZnO adheres closely to *E. coli* (Figure 3A), rather than being dispersed as ZnO NPs in the bacterial broth mixture.

In order to prove the persistence of the antibacterial effect of the new composite material, samples of Escherichia coli and Salmonella at different concentrations (10^4, 10^5) were mixed with 10 μg/mL NS-ZnO and HINS at the same time, and they were cultured at 2h, 8h, 16, 32h. Detection of bacterial activity (Figure 4A). It is found that compared with the control group, the bacteria in the experimental group have a long-term antibacterial effect, and there is no obvious bacterial growth from 2 h to 32 h. It is confirmed that the composite material has a good antibacterial and durable effect.

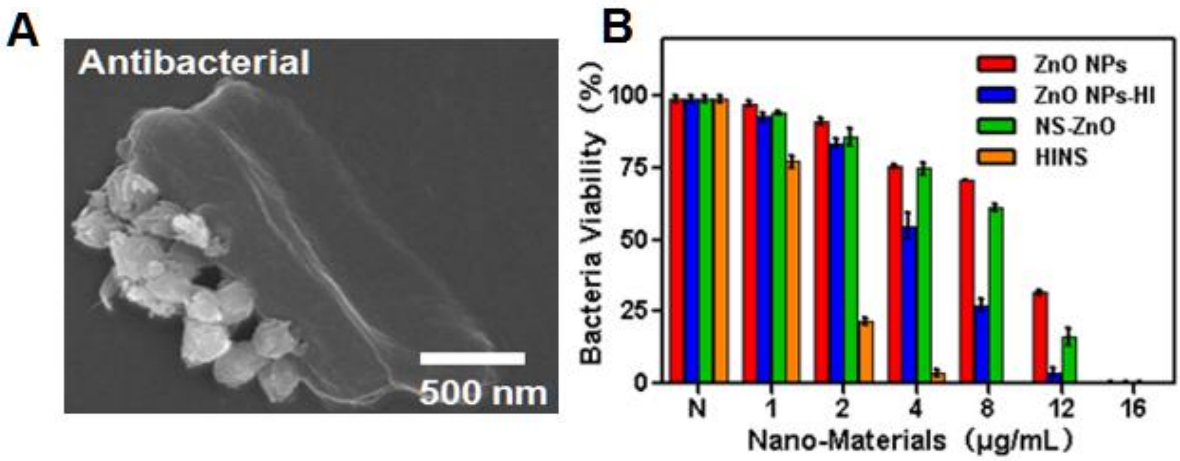

Figure 3. Antibacterials of the studied materials (ZnO NPs, ZnO NPs-HI, NS-ZnO and HINS). (A) SEM image of NS-ZnO(~200 nm) lysis bacterial (*E. coli*). (B) Effects of different concentrations of nanomaterials (ZnO NPs (~100 nm), ZnO NPs-HI, NS-ZnO (~200nm), HINS) on bacterial activity (1. 2. 4. 8. 12. 16 μg/mL); Each data value is mean ± SE of duplicate independent experiments.

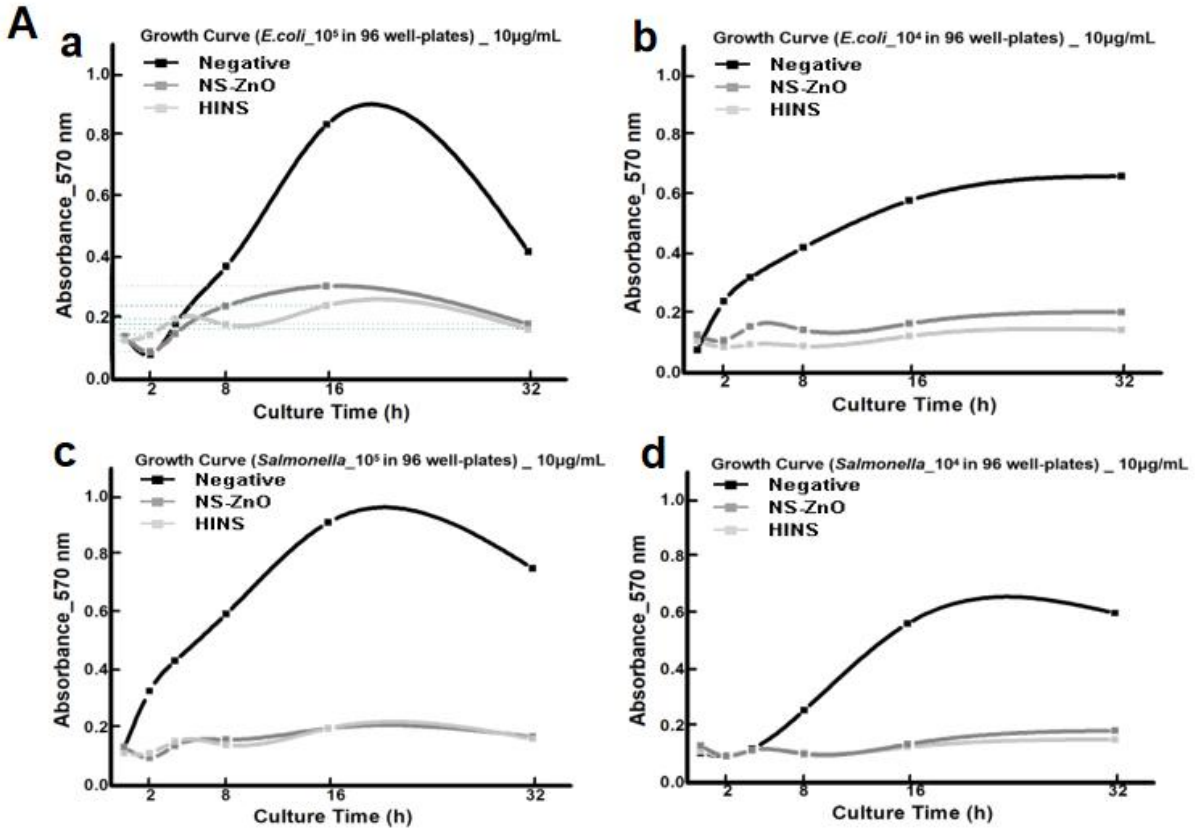

Figure 4. Antibacterials of the studied materials (ZnO NPs, ZnO NPs-HI, NS-ZnO and HINS). (A) Bacterial growth curve: ZnO NSs, ZnO NSs-HI with Negative group lived in (a)*E. coli* -10^5, (b)*E. coli* -10^4, (c)*Salmonella* -10^5, (d) *Salmonella* -10^4 all cultured in 96 well-plates. The total volume of each tube of liquid is 2 mL, and the concentration of bacterial liquid is 10 μg/ml. The absorbance value of 570 nm was measured at 2 h, 4 h, 8 h, 16 h and 32 h. The absorbance value was repeated for three times in each group and the mean value was taken.

Mealwhile，two culture methods were applied to fungi (Aspergillus fumigatus) to study the antifungal efficacy and durability of ZnO nanomaterials. Dilute a batch of Aspergillus to 4×10^4 spores/mL and set aside evenly. In the first method (Figure 5A), we mix different concentrations of ZnO nanomaterials into sterile agar and coat 200 μL of Aspergillus spores evenly. We tracked the growth of fungal colonies at 25°C for 7 days and observed that the drug concentration depends on the ratio of fungal colonies (Figure 5C). Four types of ZnO nanomaterials (ZnO NPs, ZnO NPs-HI, NS-ZnO and HINS composite materials) were added to the agar solution, with concentrations ranging from 0.1 mg/mL to 1.0 mg/mL. On the 7 th day, the proportion of fungal colonies showed that as the concentration of the drug in the agar increased, the viability of the fungal spores decreased. The presence of the HINS complex at a concentration of 0.4 mg/mL in agar showed a significant inhibitory effect and was more effective than other nanomaterials (0.6 mg/mL) at a higher concentration. In addition, the cultured agar is exposed when the concentration of HINS complex is 0.6 mg/mL (the graph in Figure 3A), which clearly proves that the effect of HINS complex not only inhibits the growth of fungal spores, but also destroys Shed them.

In another culture method test, we mixed ZnO nanomaterials with spores, and then spread them on a normal agar plate. As shown in Figure 2E, the colonies are planted in the center of the agar and scattered everywhere, so that the growth rate of fungal spores can be calculated by measuring the surface area of the colonies (Figure 5B). In this case, we record the surface area of each test colony (400 spores/culture dish, containing 0.01 mg/mL drug) every day, and its growth rate is shown in Figure 5D. It can be seen that the ZnO

nanomaterials (ZnO NPs and NS-ZnO) that are not modified by HI, the vitality of fungal spores is not inhibited over time. However, in the HI-modified nanomaterials (ZnO, NPs-HI and HINS composites), the growth rate in the first 7 days is much slower than that of other materials and reaches a stable stage in the next 7 to 14 days. This indicates that the antifungal properties of ZnO nanomaterials after HI modification are more durable, which may be caused by the activated surface energy. In addition, this confirms that the enhanced surface energy due to the HI modification is stable and durable, with high positive surface charge and high electrical conductivity (Figure 2B). In addition, SEM analysis (Figure 5C) confirmed the possible attraction of HINS complexes to invade fungal spores (surface contact) and ions (non-contact), thus proving the antifungal properties of biological HINS complexes.

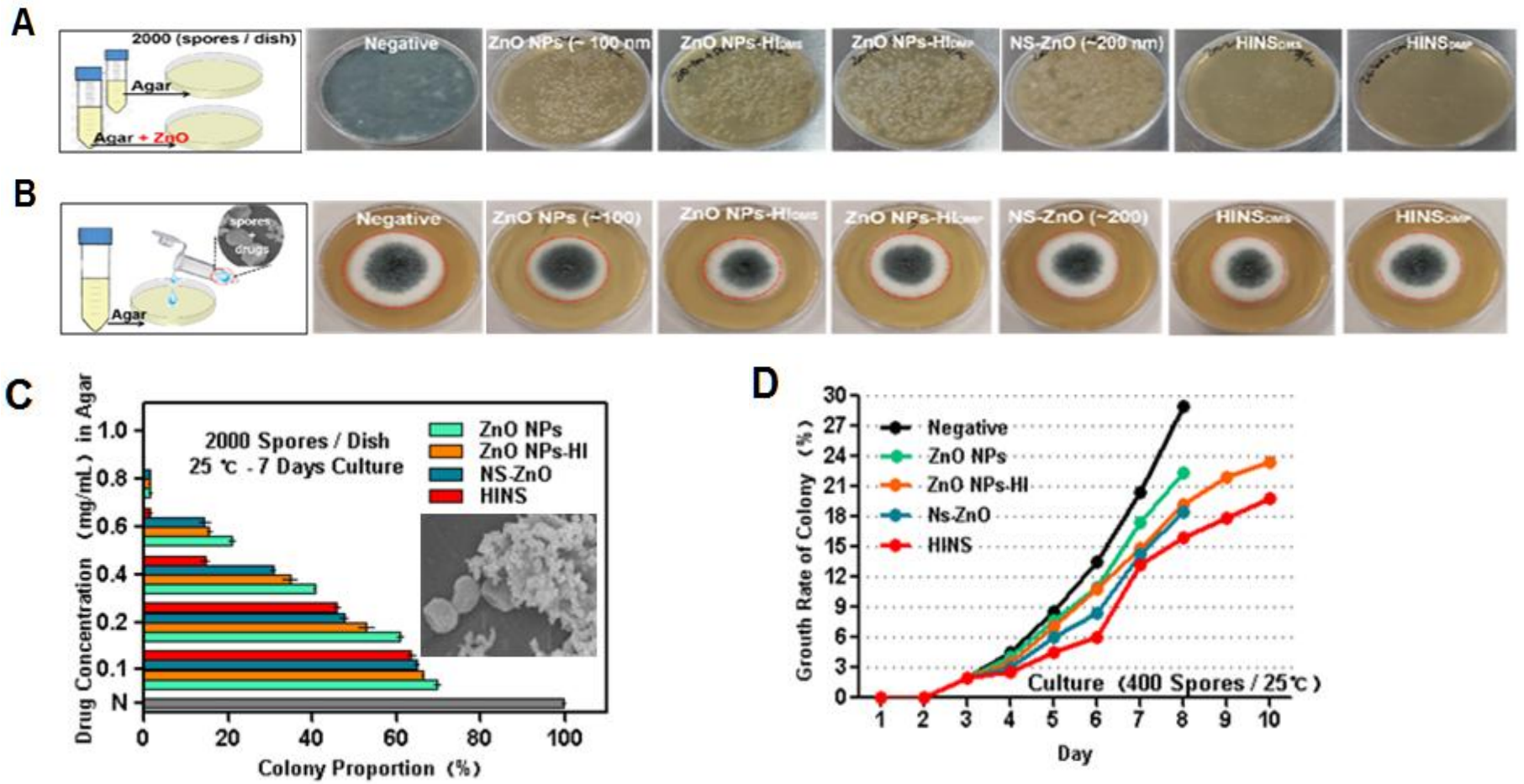

Figure 5. Antibacterials of the studied materials (ZnO NPs, ZnO NPs-HI, NS-ZnO and HINS): (A) Graphs of the 7 day-cultured Aspergillus colony with ZnO nanomaterials at 0.6 mg/mL. (B) Graphs of the Day 4 cultured Aspergillus colony with ZnO nanomaterials. (C) The proportion summary of treatment of Aspergillus colony at different concentrations (0.1–1.0 mg/mL) of ZnO nanomaterials. (D) The day–growth rate of Aspergillus colony as tracked for 10 d (Each data value indicates ± SE of duplicate independent experiments).

At the same time, I tested a study on HINS and antifungal drugs (Itraconazole). After testing the efficiency of itraconazole, we chose a medium concentration (6 μg/mL) as the precursor to check Whether there is a synergistic effect during the interaction of 0.1 mg/mL ZnO nanomaterials. The diameter of the Aspergillus colony was recorded every day and displayed in Figure 6A (Aspergillus bacteria chart on day 6) and Figure 6B (Growth trend chart). The results showed that the cooperation not only enhanced the antifungal efficacy, but also showed a sustained inhibitory effect after 9 days of cultivation. When the inhibition rate of ZnO NPS-HI was 35%, the HINS complex showed 70% inhibition on the 5th day. Compared with the negative group (untreated), the downline lining growth rate of the treated Aspergillus colony group conformed to the growth pattern, showing the advantages of the HINS complex in prolonging the administration time and reducing the administration frequency. After 6 days of cultivation with pure itraconazole and pure ZnO nanomaterials, the growth rate increased rapidly, which means that the pure drug lost its efficacy in inhibiting the growth of new spores. However, on the 6th day, the synergistic inhibitory effect between the HINS complex and the antibiotic itraconazole reached almost 90%, which is quite a significant enhancement, indicating that the HINS complex solution can be used as a protective buffer or solvent. In order to reduce the loss caused by solubility, it adheres to the container wall and prolongs the action time. The evaluation of its biocompatibility and toxicity will affect further medical applications, such as ointment smears, oral and intravenous drug delivery systems.

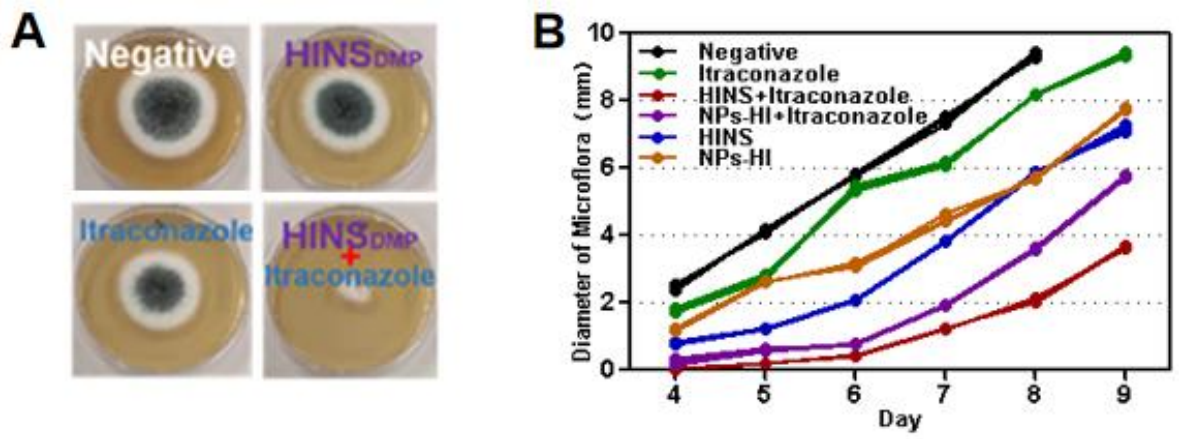

Figure 6. Antibacterials of the studied materials (ZnO NPs, ZnO NPs-HI, NS-ZnO and HINS) (A) Graphs of the Aspergillus colony. (B) Daily record of the diameter of Aspergillus colony, tracking for 9 d, 400 spores/dish (ZnO nanomaterials: 0.1 mg/mL, Itraconazole: 6 μg/mL, in 50 μL), 25 , 7 d of culture. Each data value indicates ± SE of duplicate independent experiments.

3.3. Mechanism and synergistic antibiotic effect of HINS composite

As shown in Figure 7A, the study put forward the antibacterial hypothesis mainly due to (1). the massive production of ROS, (2). The release of Zn ions and (3). the physical properties of HINS. Studies have shown that semiconductor nanomaterials cause oxidative stress through effective antioxidant reactions in the bacteria environment. When performing the DCFDA-ROS kit test (Figure 8A), Compared with the control group, ZnO-related nanomaterials can generate a large amount of ROS, which is about 1.6 to 2 times that of culture without materials. It is confirmed that there is indeed a large amount of ROS production, and related research papers point out that the large amount of ROS and the environment can indeed effectively affect the activity of normal cells and kill cells.

In order to study the effect of ions on the growth of fungi, we designed an external ion-assisted experiment. The method is to add salt solution as high concentration (10 M, 10 μL) and low concentration (0.1 M, 10 μL) effectors. In this case, the main purpose is to provide Zn^{2+} ions through $Zn(NO_3)_2$ and $ZnCl_2$, while setting Na_2CO_3, NaCl, $MgSO_4$ and $(NH_4)_2CO_3$ to eliminate interference. We cultivated 1,000 Aspergillus spores per petri dish at 37°C to simulate the biological environment (Figure 8B). The colonies on day 3 are summarized in Fig. 3C, and the results show that: (1). Zn^{2+} ions have an important effect against fungal spores, not Na^+, Mg^{2+} or NH_4^+ ions, and when supplemented with high molar (10 M) Zn^{2+}, Its efficacy is almost twice that of pure NS-ZnO. (2). The reduction effect of salt solution in low molar (0.1 M) reveals the self-protective properties of fungal spores. We also tested the effect of ions on HINS composites and found that it is not as obvious as NS-ZnO.

This may be due to the covalent covalent bond between the imido acid ester functional group and the acid radical ion (which can extend the activity of Zn^{2+}).

Similarities appeared in the pH effect, we adjusted the broth with high acid, which is the antifungal effect of HINS. Composite materials are eliminated (Figure 8C). However, the NS-ZnO and HINS composite material still retains its antifungal properties when the pH is tested in agar medium. Under human conditions, the three simulated pH values are set to pH 7.5 (blood), pH 4.5 (intestine) and pH 2.5 (stomach). The excellent antifungal activity of the HINS complex was demonstrated in each pH gradient, which confirmed that the HINS complex may be a potential ointment on the surface of endothelial wounds (Figure 8D). The sustained activity in the neutral blood pH medium also implies the possibility of safe intravenous injection of drugs.

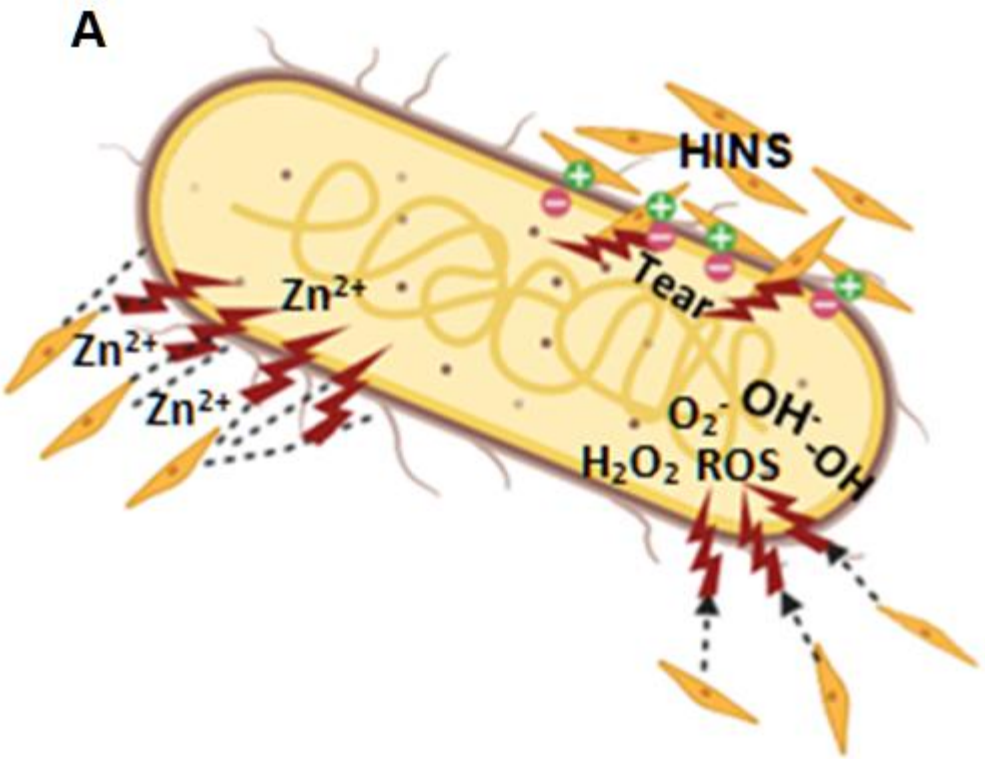

Figure 7. Study on antibacterial mechanism of new HI-compound zinc oxide. (A) Scheme of the hypothesized antifungal mechanism of HINS composite and proposed synergistic effect with traditional antibiotic itraconazole.

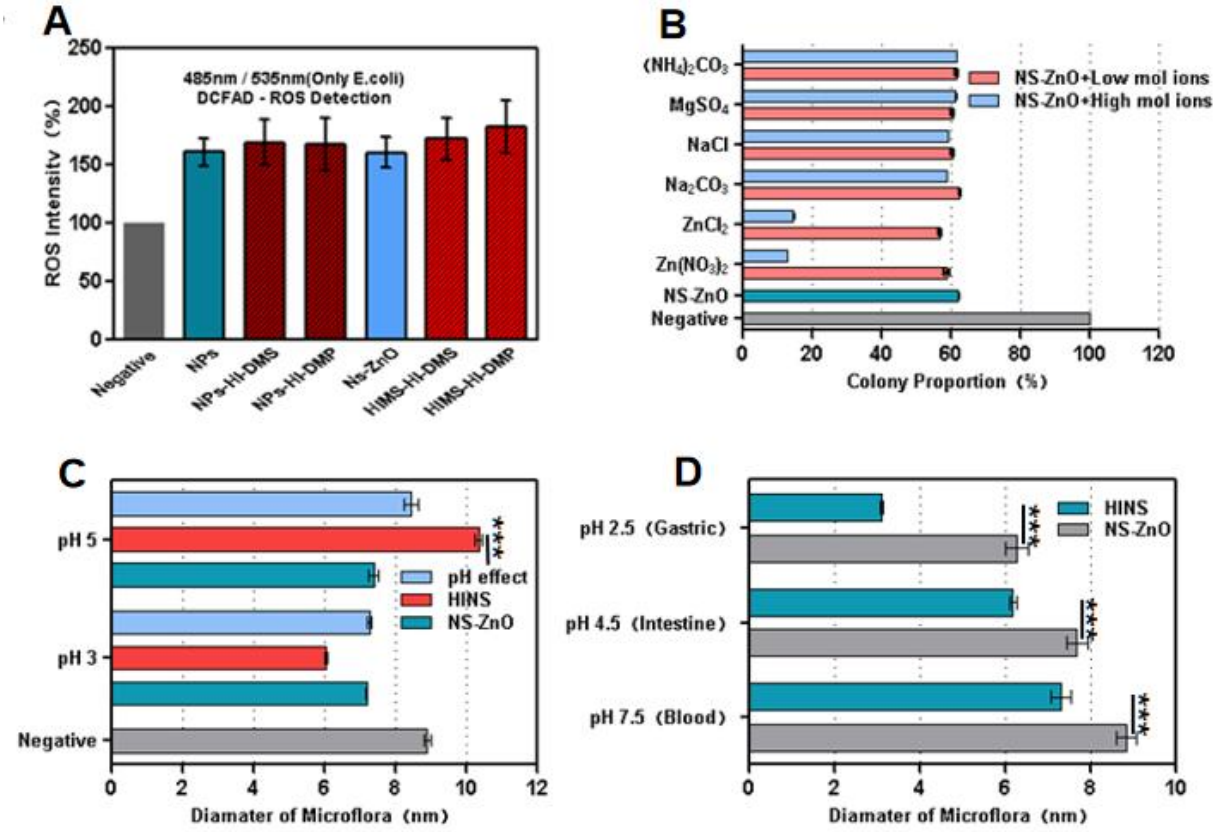

Figure 8. Study on antibacterial mechanism of new HI-compound zinc oxide. (A) Cellular ROS detection assay of ZnO nanomaterials with *E.coli* culture, DCFAD kit in 485 nm/535 nm (B) Ion effect (Zn^{2+}, Mg^{2+}, Na^{+}, NH^{4+} and acid radical ions) on the antifungal properties of the NS-ZnO by colony formation method, 1000 Aspergillus spores/dish, (0.1 mg/mL, 50 μL) at 37 ℃, after 3 d of culture. (C) Acid effect (H^{+}) on the antifungal properties of the NS-ZnO and HINS composite in broth. (D) Modeling of the internal environment with pH medium (blood:7.5, intestine:4.5 and gastric:2.5) for studying the practical effect of HI modification on the antifungal properties.

3.4. *In vitro* study of HINS composite

For ZnO nanomaterials modified by HI (DMS, DMP), it is necessary to study their biocompatibility. The purpose is to research that may be applied to clinical trials in the future. Here we used two kinds of cells: L929 mouse-derived normal cells and HCT-116 human-derived cancer cells as the research object. After different concentrations of nanomaterials (2, 4, 6, 8 μg/mL) were co-cultured with cells, the cytotoxicity was observed by MTT method (Figure 9A-B). The results confirmed that in the two types of cells, their activity can be slightly affected by the ZnO composite material, and we think it may be related to the effect of the ROS generated by the nanomaterial on the cell activity. However, the slight effect does not have obvious cytotoxicity, so it can be applied to future clinical research.

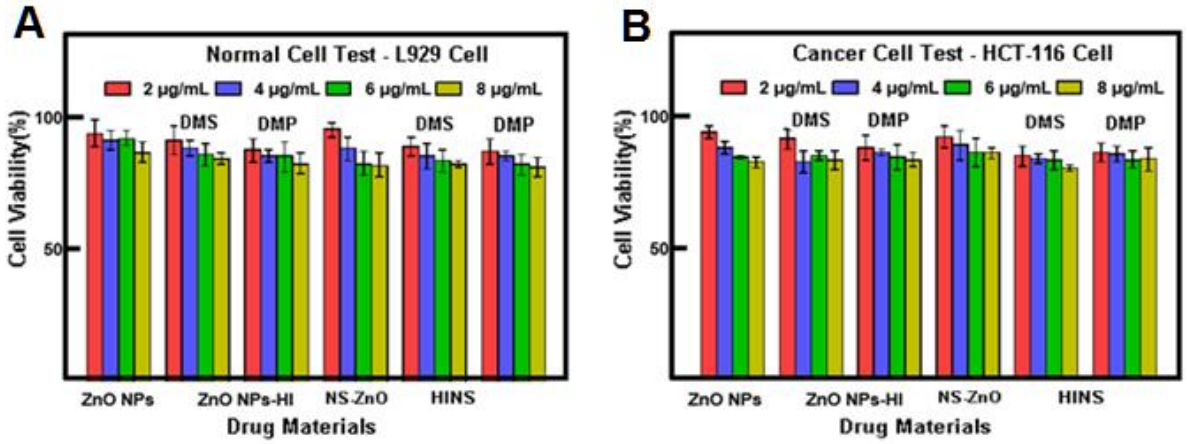

Figure 9. Study ofbiocompatibility and toxicity of HINS composite *in vitro*cell test. (A) Comparison of toxicity of nanomaterials (ZnO NPs, ZnO NPs-HI, NS-ZnO and HINS) to L929 mouse derived normal cells at different concentrations (2, 4, 6, 8 μg/mL).(B)Comparison of toxicity of nanomaterials (ZnO NPs, ZnO NPs-HI, NS-ZnO and HINS) to Human HCT-116 cancer cells at different concentrations (2, 4, 6, 8 μg/mL). Each experimental group was cultured in 15,000 cells per well with the material at 37 for 24 hours. MTT assay detection. Each data value indicates ± SE of duplicate independent experiments.

3.5. *In vivo* study of HINS composite

I propose that HINS has a spindle-shaped physical structure due to its nano-scale size, low toxicity in cells and good biocompatibility. It can smoothly pass through blood vessels and reach the diseased parts of the body to kill pathogens. (Figure 10A)

So next, I evaluated the in vivo toxicity of HINS composite materials in accordance with the requirements of the local ethics committee. After intravenous injection of the HINS complex, clinical signs of toxicity, such as tremor, convulsions, salivation, nausea, vomiting, diarrhea, and weight changes in mice were recorded within 14 days. There was no death at the two doses. In the low-dose and high-dose administration groups, there was no significant change in the body weight or toxicity symptoms of any mice (Figure 10.B-C). Study on blood biochemistry in mice (Figure 11A. a-d) shows that the lack of large waves of alanine aminotransferase (ALT) or aspartate aminotransferase (AST) is a reliable test for liver damage. Bile tests for bilirubin, blood urea nitrogen (BUN) and creatinine (Crea) are used for the normal work of the kidneys. The total protein (TP), albumin, and albumin/globulin ratio (A/G) are stable, indicating a healthy state. These proteins can be used to estimate the qualitative changes in lipoproteins and prevent blood leakage from the blood vessels; total cholesterol (T-Chol), triglycerides (TG), glucose and phosphorus have normal wave changes. All these results indicate that there are no signs of toxicity in mice treated with low-dose or high-dose HINS complexes by intravenous administration in vivo. These findings indicate that HINS composite materials are relatively safe for use as antibiotics in biomedical applications.

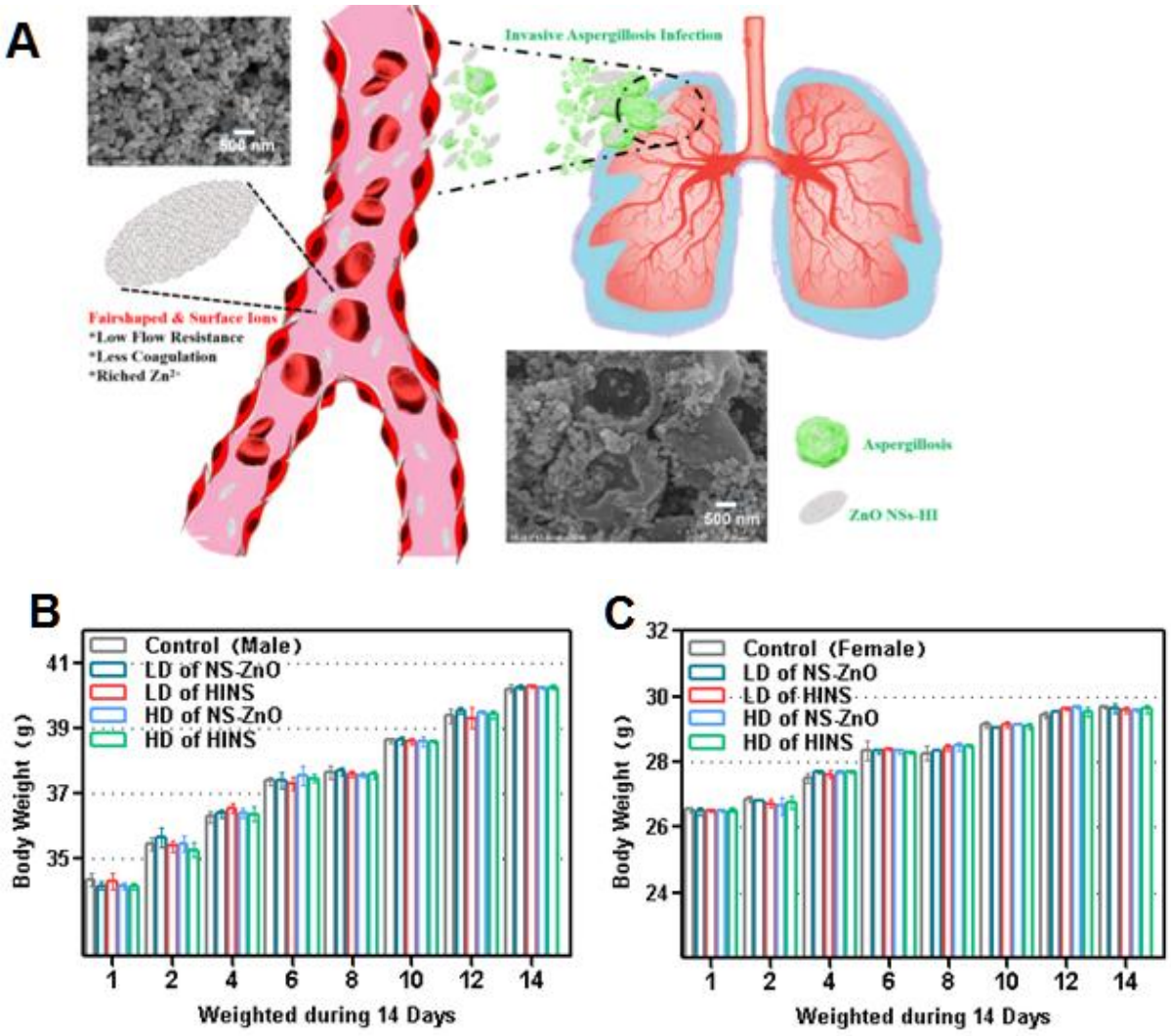

Figure 10. Study of biocompatibility and toxicity of HINS composite in vitro mice test. (A) Schematic diagram of new composite nanomaterials entering blood circulation in the body. (B-C) Body weight changes of the mice treated with LD and HD of NS-ZnO or HINS composite by intravenous administration, monitored for 14 d, A: male; B: female. (Each data value indicates ± SE (n = 10 mice per group) Abbreviations: LD-low dosage; HD-high dosage).

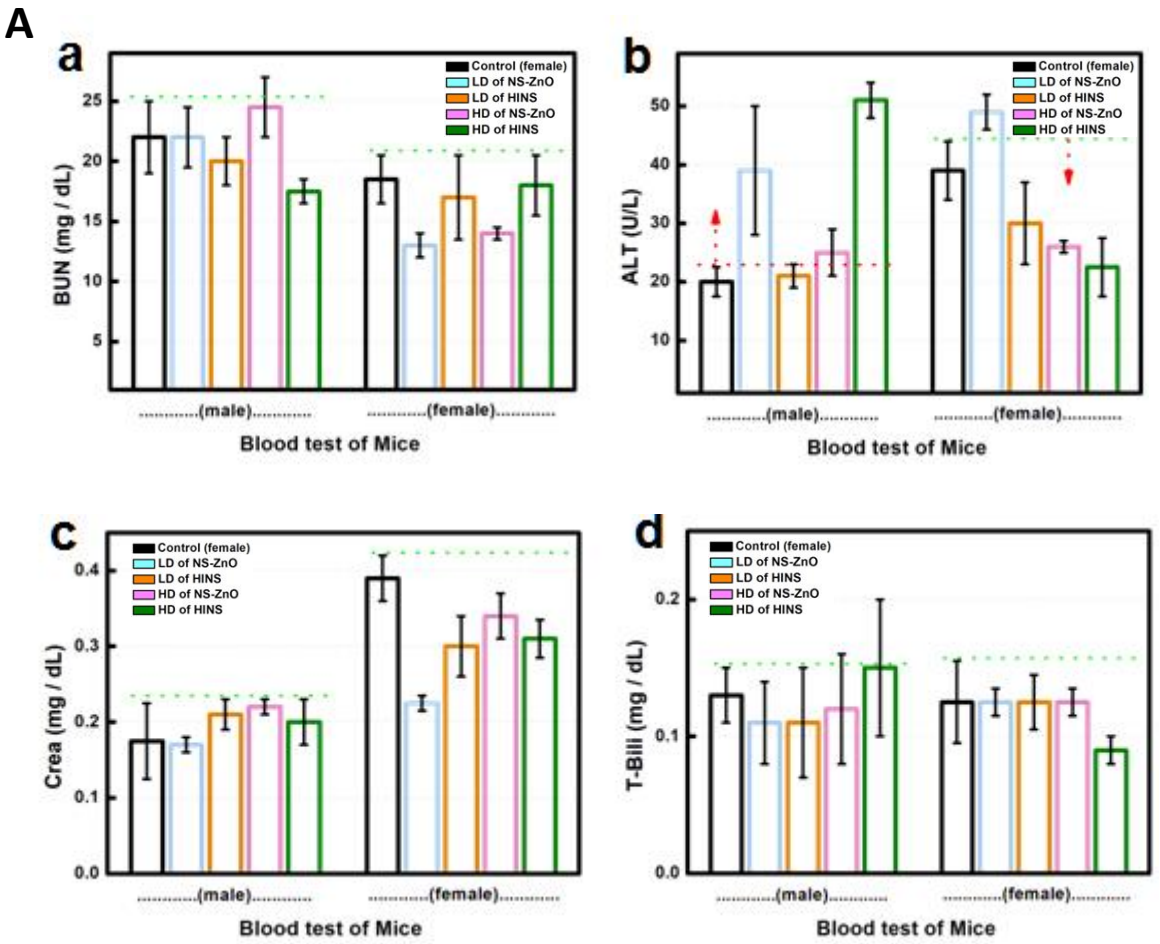

Figure 11. Study of biocompatibility and toxicity of HINS composite in vitro mice test. (A) Blood index test results of nanomaterials entering the mice body. (a) Blood urea nitrogen BUN. (b) Alanine aminotransferase ALT. (c) Creatinine entering the blood Crea. (d) Total bilirubin T-Bil. The LD-HINS and HD-HINS composites were studied, and the data values are all mean ± SE. Abbreviations: LD-low dose; HD-high dose. Each data value indicates ± SE. (n = 5 mice per group).

CHAPTER 2 - Diagnostic application of BP-NIR-HI system

3.6. Procedure and chemical characterization of Black phosphorus nanoparticles

First, we use commercial black phosphorous nanosheets (Figure 12A), which are sonicated to disperse them into black phosphorous nanoparticles of uniform size. The SEM test showed that the black phosphorus nanoparticles have good dispersibility (Figure 12B). Moreover, the size of the material is mainly about 50-100nm. Such nano-scale particles are more conducive to being dispersed in the solution and mixed with pathogens, so that the maximum efficiency of cell lysis can be achieved during the laser irradiation process. Then, in the black phosphorus solution after ultrasonic dissolution in the aqueous solution, the element composition test of the chemical bond (Figure 12C) proves that the black phosphorus is not degraded in the aqueous solution, but exists in a large amount, so that the photothermal property has the best heating effect. After we have been irradiated by the laser, we recorded the heating effect of black phosphorus at a concentration of 1 mg/ml with an infrared temperature detector. It can rise from 39°C to 62°C in one minute (Figure 12D), and this temperature it can promote the decomposition of pathogen cells to release DNA, and the temperature rises rapidly. In subsequent studies, we compared the heating efficiency under different black phosphorus concentrations and laser currents. Obtain the temperature growth curve of the difference between black phosphorus and current over time, and after stopping the black phosphorus heating, the temperature can be quickly reduced (Figure 13A). So that after the DNA release temperature is reached, the temperature can be quickly reduced by turning off the laser. It is to prevent heat damage to DNA.

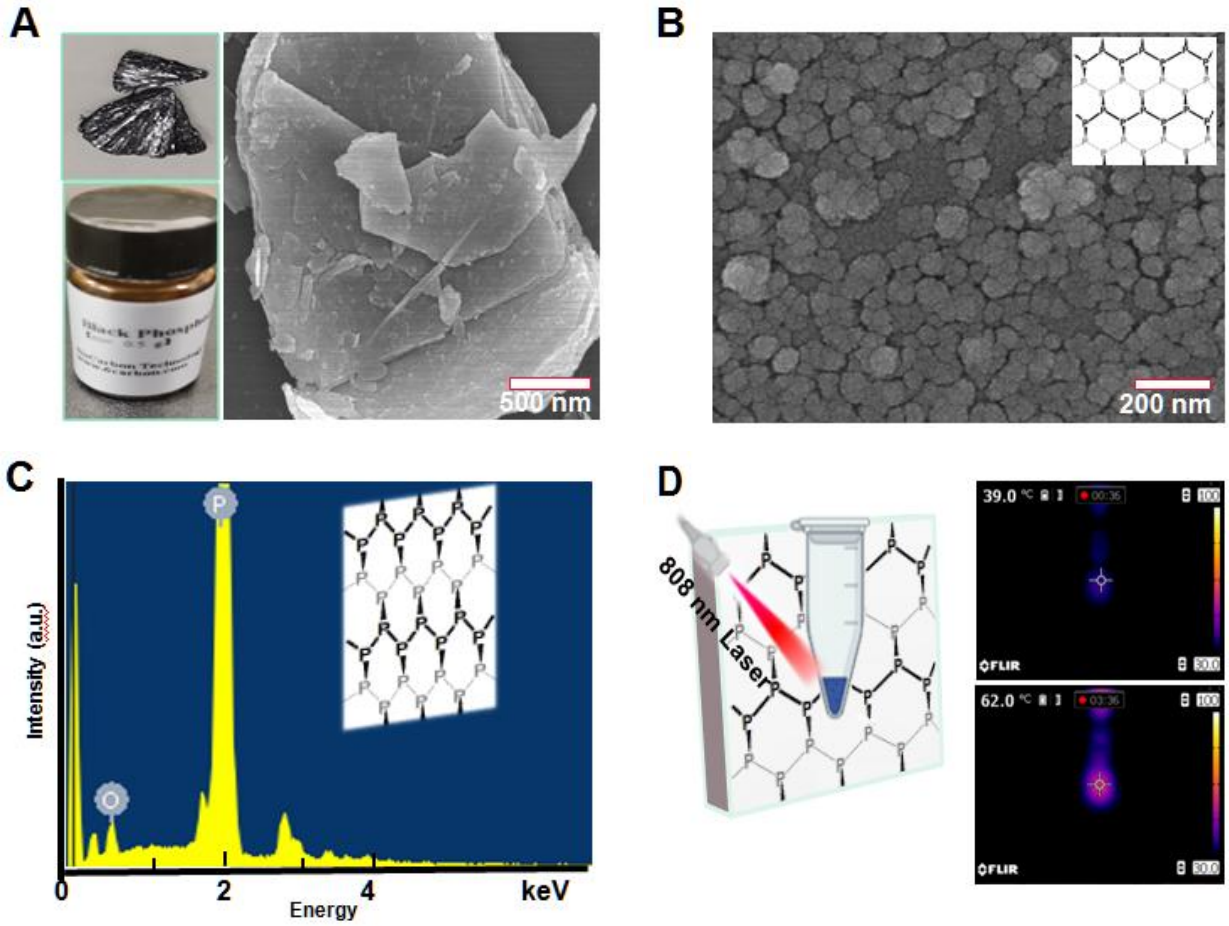

Figure 12. Characterization of black phosphorous Multilayer and nanosheet. (A) The physical image and SEM image of commercial solid black phosphorous. (B) SME image of black phosphorous nanosheets after ultrasonic 4h in water bath (50~100nm). (C) Diagram of the valence bond structure of black phosphorous nanosheets. (D) Infrared thermostat records the actual temperature rise of BP nanosheets irradiated by 808nm laser.

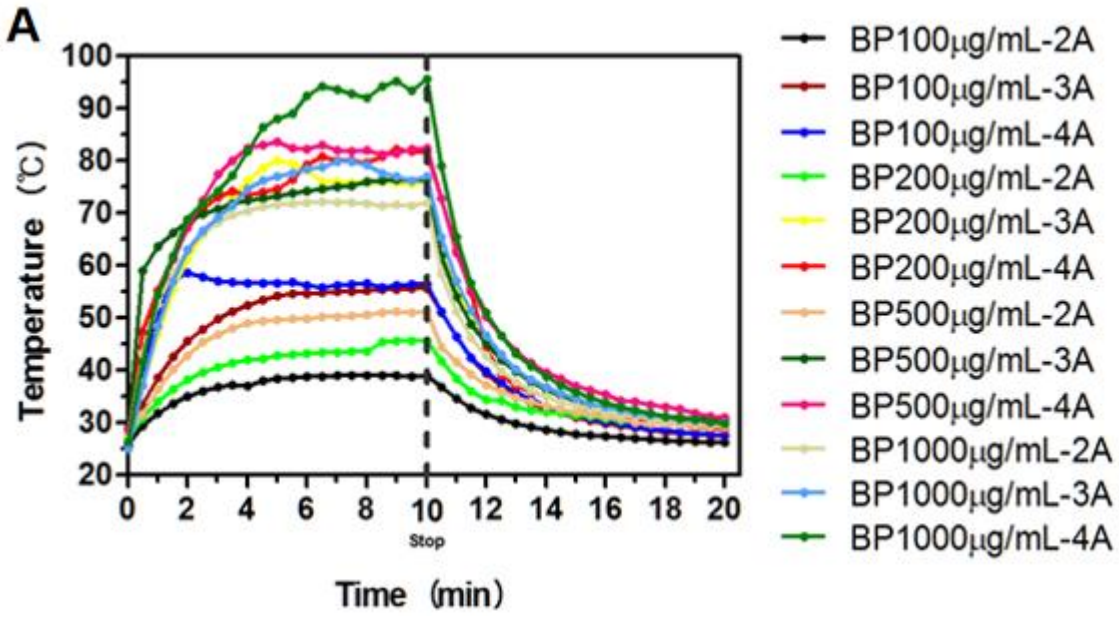

Figure 13. Characterization of black phosphorous Multilayer and nanosheet. (A) Comparison of temperature rise and fall of BPNs with different concentrations after 808nm laser irradiation with different currents, all experimental groups at 10 minutes Stop irradiation.

3.7. Performance evaluation of DNA extraction using the BP-NIR-HI method

In order to test how influence the two methods have on the content of DNA extraction. After the *E. coli* sample was extracted by the BP-NIR-HI system (Figure 14), it was compared with the DNA sample extracted by the QIAGEN kit. Real-time PCR detection was performed, and the effect of Ct value with different BP concentration and HI (DMS) concentration was obtained (Figure 15A). The results confirmed that compared with DNA obtained by DW and QIAGEN kit methods, the Ct value was significantly lower, and the best effect was in the group of 500 μg/mL BP and 50 μL 100 μg/mL HI. And the BP200-HI20 group also showed better results than the other groups. At the same time, it was observed after the Nano drop test that this group also had the best DNA concentration content (Figure 15B). Meanwhile, the BP200-HI20 group also showed better results compared with other groups, which also confirmed that HI (DMS) plays a vital role in DNA extraction and enrichment. The statistical comparison of the data in each group also confirmed that $P<0.01$ has an extremely significant difference.

Objective to compare the effects of single factor BP, Laser and HI on DNA extraction and enrichment, and compare the DNA samples extracted by different single factor two factor experimental groups and BP-NIR-HI by Real-time PCR and compare the Ct values (Figure 15C). The results It also shows that in the case of BP, NIR and HI co-existing, the fluorescence detection threshold can be reached with fewer amplification cycles, so it can be proved that this method obtains higher DNA content than other groups.

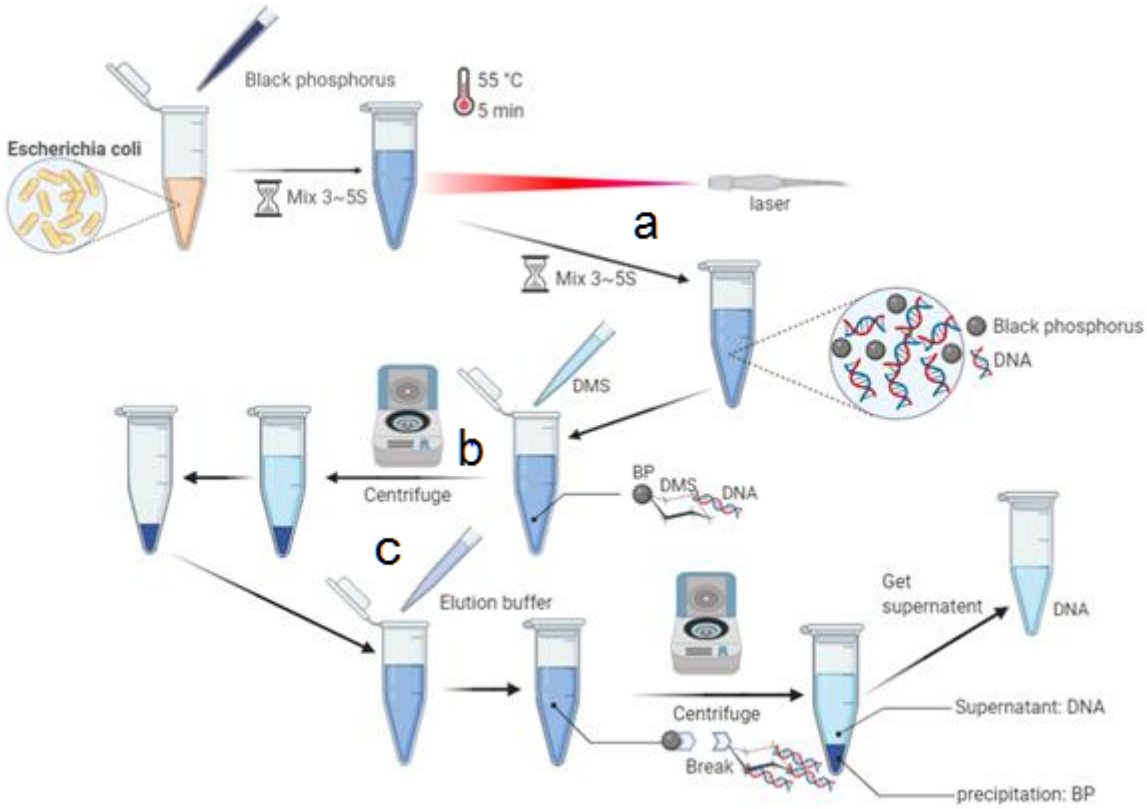

Figure 14. Flow chart of DNA extraction by BP-NIR-HI system.

(a) First, the 200 μL 1×10^5 *E.coli* sample to be tested is combined with 500 mg/mL 200 μL black phosphorous nanosheets solution, and the sample is irradiated with a 3A current intensity NIR laser to increase the temperature of the system to 55 and then keep the temperature for 5 minutes.

(b) Then, after vortex, add 50 μL 100 mg/mL HI(DMS) to the test tube and mix for 1~2 min, then centrifuge at 13000 rpm for 1 min to remove the supernatant.

(c) Last, Add 100 μL of Elution buffer pH 10.6, mix, and centrifuge at 13000 rpm for 1min to obtain the supernatant, which is the solution containing DNA.

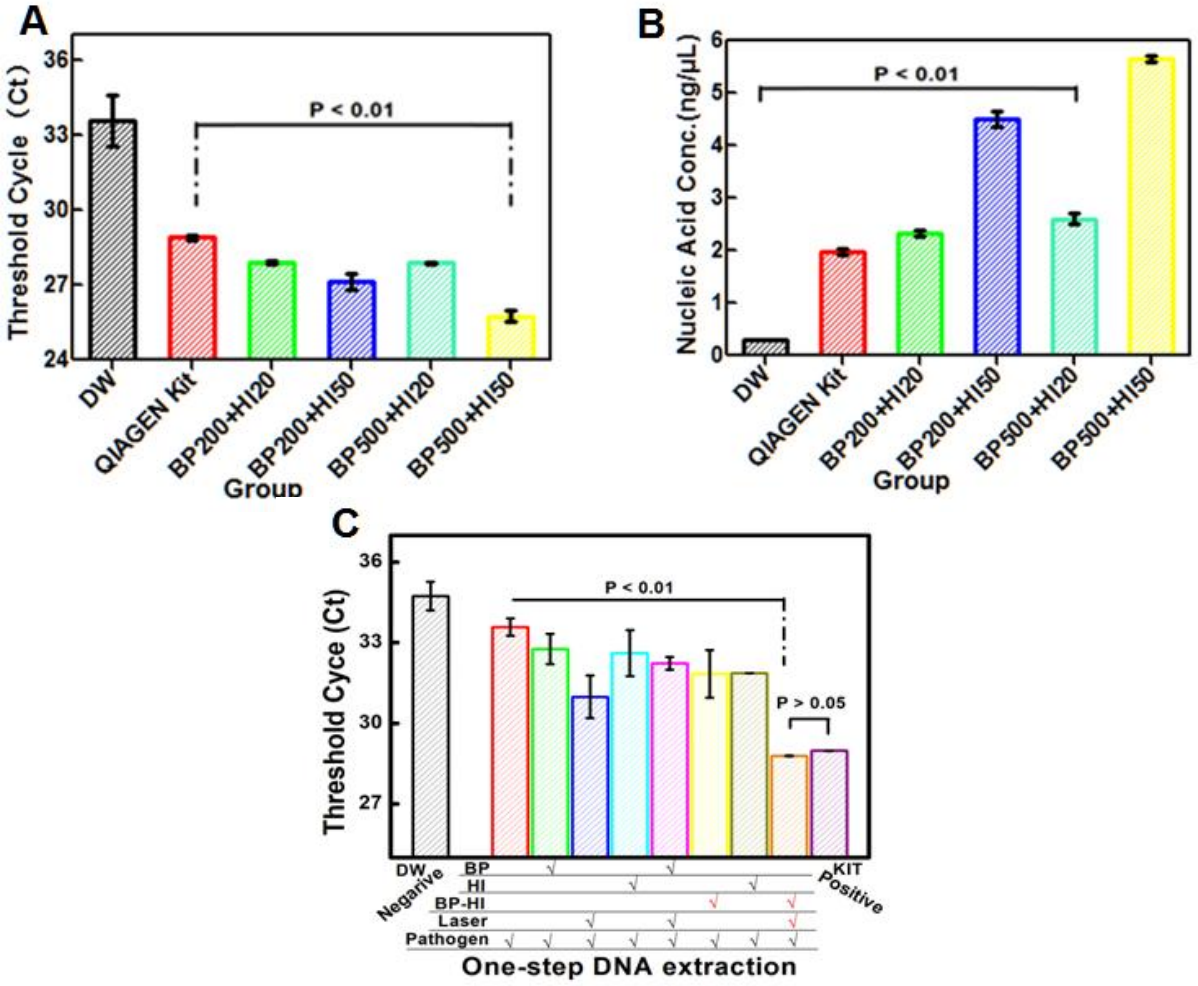

Figure 15. Performance evaluation of DNA extraction using the BP-NIR-HI method. (A)Experimental group (different concentrations of BP (200 μg/mL, 500 μg/mL) and different concentrations of HI (20 μL, 50 μL)) Compared with the Ct value graph of the control group DW and QIAGEN Kit after Real-time PCR amplification. (B)Nucleic acid concentration results of Nano-drop after DNA extracted from DW and QIAGEN kit and different concentrations of BP-NIR-HI system. (C)Ct value comparison of the BP-NIR-HI group with the single- factor group BP, HI, Laser and the double-factor group BP- HI, BP-Laser, HI-Laser and the control group DW and QIAGEN Kit group after DNA amplification by Real time PCR. Each data value indicates ± SE of duplicate independent experiments.

3.8. Study on the mechanism of DNA extraction by BP-NIR-HI system

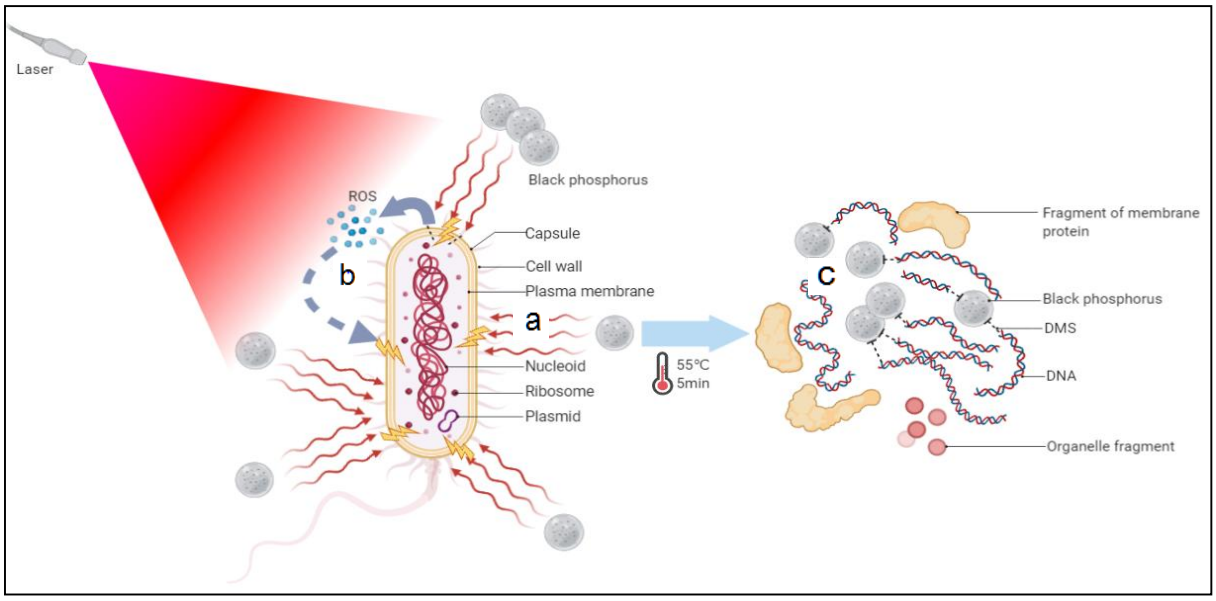

Figure 16. Schematic diagram of BP-HIR-HI system for DNA extraction.

For the mechanism by which the BP-NIR-HI system can perform DNA extraction, we propose several hypotheses(Figure 16). First, after being irradiated by laser, black phosphorus will produce high temperature to inactivate the surface membrane protein of *E. coli* and cleave the cells. Next, after the black phosphorus is irradiated by laser, high temperature stimulates *E. coli* itself to produce a large amount of ROS, and ROS will affect and destroy the surface membrane and cell wall of the bacteria. Last, DMS(HI) binds the black phosphorus to DNA fragments, allowing more DNA to aggregate and be segregated by centrifugation. Compared with the traditional QIAGEN Kit dissolution and elution method, DNA damage can be minimized.

4. DISSCUSSION

In this study, a new simplified method was used to synthesize a spindle shaped zinc oxide with a size of about 200nm. Compared with commercial zinc oxide, it has better anti-fungal and anti-bacterial activity. Then, for the first time, the surfactant DMS and DMP were combined on the surface of ZnO to form the composite NS-ZnO (~200nm) to obtain the best antibacterial effect and non-toxicity in vivo. At the same time, we also observed that the HINS (~200nm) composite was closely bound to the membrane of the pathogen, which destroyed the morphology of the membrane of the pathogen. Through many experiments, we have demonstrated several possible mechanisms by which HINS (~200nm) can enhance antibacterial activity: (1). After modified by DMS and DMP, the surface charge of composites has strong positive charge. The surface charge of microorganisms is negative. It is beneficial for more microorganisms to bond to the composite due to the charge attraction. (2) The new composite ZnO has spindle elliptic shape and porous structure, and has relatively large specific surface area, which is more conducive to adsorbing more microorganisms. (3) The generation of reactive oxygen species is increased, and the duration is longer. Compared with other ZnO materials, HINS (~200nm) composite material can improve the activity of reactive oxygen species for a longer time at both cellular and non-cellular levels. (4) Excessive zinc ion (Zn^{2+}). When the composite binds to the pathogen, Zn^{2+} can directly destroy the cell wall. In addition, we assessed the toxicity of ZnO to mice after oral administration. Although further studies were expected to fully determine the safety of HINS (~200nm) in mice and humans, we observed that the composite was safe at experimental doses for two weeks.

Compared with the control group, they had normal organ weight and normal blood tests.

Finally, I systematically investigated the synergism of HINS (~200nm) composite with existing an antifungal agent (Itraconazole). This antifungal agent alone has many limitations, such as high toxicity, poor solubility, sensitivity to pH, and severe side effects in cancer and transplant patients. The antifungal effect of HINS(~200nm) combined with the above two antifungal drugs was significantly enhanced than that of single treatment. Our results show that this new nontoxic nano zinc oxide composite can be used as an antibiotic in the clinical environment of fungi. Therefore, we believe that this new composite material can be used as a good anti-bacterial and fungal drug in medicine, food, environment, and other aspects with a good application prospect.

For another study. It was confirmed in the study of extracting DNA using the photothermal properties of black phosphorus. Compared with the traditional commercial QIAGEN kit, the BP-NIR-HI system can obtain higher concentration of DNA. At the same time, the system is the result of BP, NIR laser irradiation, and HI modification, and a single factor cannot have a good result for DNA extraction. As for the mechanism hypothesis of this system, it is currently believed to be mainly due to (1). BP photothermal property increases the temperature in a short period of time to inactivate and lyse *E. coli* cells. (2). Photothermal produces a large amount of ROS and also causes cell destruction to release a large amount of release DNA. (3). HI can make DNA and BP produce chemical bond connection, which is conducive to DNA enrichment.

BP as a representative of a new type of two-dimensional material, has been proven to be used in drug-carrying systems, and has good photothermal properties in anti-tumor

biomedical research. And mine is about BP's research on DNA extraction, which makes it possible for BP to study in the medical field of diagnosis and detection in the future and has a good application potential. It laid the foundation for the subsequent research on diagnosis.

5. REFERENCE

1. Sun Y, Li S, Zhang Y, et al. Tetrahedral Framework Nucleic Acids Loading Ampicillin Improve the Drug Susceptibility against Methicillin-Resistant Staphylococcus aureus[J]. *ACS Applied Materials & Interfaces*, 2020, 12(33): 36957-36966.
2. Prestinaci F, Pezzotti P, Pantosti A. Antimicrobial resistance: a global multifaceted phenomenon[J]. *Pathogens and global health,*2015, 109(7): 309-318.
3. Vincent J L, Sakr Y, Singer M, et al. Prevalence and outcomes of infection among patients in intensive care units in 2017[J]. Jama, 2020, 323(15): 1478-1487.
4. Zhao Y, Guo Q, Dai X, et al. A Biomimetic Non Antibiotic Approach to Eradicate Drug Resistant Infections[J]. *Advanced Materials*, 2019, 31(7): 1806024.
5. Monk B C, Goffeau A. Outwitting mμLtidrug resistance to antifungals[J]. *Science*, 2008, 321(5887): 367-369.
6. Vidallon M L P, Teo B M, Cao X, et al. rsc. li/chemcomm[J]. *Chem. Commun*, 2020, 56: 13895-13906.
7. Musher D M, Abers M S, Corrales-Medina V F. Acute infection and myocardial infarction[J]. New England Journal of Medicine, 2019, 380(2): 171-176.
8. Ding X, Wang A, Tong W, et al. Biodegradable Antibacterial Polymeric Nanosystems: A New Hope toCope with MμLtidrug Resistant Bacteria[J]. *Small*, 2019, 15(20): 1900999.
9. Madannejad R, Shoaie N, Jahanpeyma F, et al. Toxicity of carbon-based nanomaterials: Reviewing recent reports in medical and biological systems[J]. Chemico-biological

interactions, 2019, 307: 206-222.

10. Wang S, Gao Y, Jin Q, et al. Emerging antibacterial nanomedicine for enhanced antibiotic therapy[J]. *Biomaterials Science*, 2020.

11. Howard K C, Dennis E K, Watt D S, et al. A comprehensive overview of the medicinal chemistry of antifungal drugs: perspectives and promise[J]. *Chemical Society Reviews*, 2020, 49(8): 2426-2480.

12. Piva R H, Rocha M C, Piva D H, et al. Acidic dressing based on agarose/Cs2. 5H0. 5PW12O40 nanocomposite for infection control in wound care[J]. *ACS applied materials & interfaces*, 2018, 10(37): 30963-30972.

13. Cheeseman S, Christofferson A J, Kariuki R, et al. Antimicrobial Metal Nanomaterials: From Passive to StimμLi Activated Applications[J]. *Advanced Science*, 2020, 7(10): 1902913.

14. Guo L, Wang H, Wang Y, et al. Organic Polymer Nanoparticles with Primary Ammonium Salt as Potent Antibacterial Nanomaterials[J]. *ACS applied materials & interfaces*, 2020, 12(19): 21254-21262.

15. Qi G B, Zhang D, Liu F H, et al. An "On Site Transformation" Strategy for Treatment of Bacterial Infection[J]. *Advanced Materials*, 2017, 29(36): 1703461.

16. Wei W, Rosenkrans Z T, Luo Q Y, et al. Exploiting Nanomaterial Mediated Autophagy for Cancer Therapy[J]. *Small methods*, 2019, 3(2): 1800365.

17. Kim I, Viswanathan K, Kasi G, et al. ZnO nanostructures in active antibacterial food packaging: Preparation methods, antimicrobial mechanisms, safety issues, future prospects, and challenges[J]. *Food Reviews International*,2020: 1-29.

18. Musselman K P, Muñoz-Rojas D, Hoye R L Z, et al. Rapid open-air deposition of uniform, nanoscale, functional coatings on nanorod arrays[J]. *Nanoscale horizons*, 2017, 2(2): 110-117.

19. Zhang R, Jiang J, Zhou J, et al. Biofunctionalized "Kiwifruit Assembly" of Oxidoreductases in Mesoporous ZnO/Carbon Nanoparticles for Efficient Asymmetric Catalysis[J]. *Advanced Materials*, 2018, 30(11): 1705443.

20. Tanino R, Amano Y, Tong X, et al. Anticancer activity of ZnO nanoparticles against human small-cell lung cancer in an orthotopic mouse model[J]. *MolecμLar cancer therapeutics*, 2020, 19(2): 502-512.

21. Bai X, Li L, Liu H, et al. Solvothermal synthesis of ZnO nanoparticles and anti-infection application in vivo[J]. *ACS applied materials & interfaces*, 2015, 7(2): 1308-1317.

22. Lakshmeesha T R, Kalagatur N K, Mudili V, et al. Biofabrication of zinc oxide nanoparticles with Syzygium aromaticum flower buds extract and finding its novel application in controlling the growth and mycotoxins of Fusarium graminearum[J]. *Frontiers in microbiology*, 2019, 10: 1244.

23. Li M, Zhu L, Lin D. Toxicity of ZnO nanoparticles to Escherichia coli: mechanism and the influence of medium components[J]. *Environmental science & technology*, 2011, 45(5): 1977-1983.

24. Hermanson G T. et.al [M]. *Academic press*, 2013.

25. Liu H, Luan Y, Koo B, et al. Cucurbituril-based reusable nanocomposites for efficient molecμLar encapsμLation[J]. *ACS Sustainable Chemistry & Engineering*, 2019, 7(5):

5440-5448.

26. Liu H, Noh G S, Luan Y, et al. A sample preparation technique using biocompatible composites for biomedical applications[J]. *MolecμLes*, 2019, 24(7): 1321.

27. Liu H, Zhao F, Koo B, et al. Dimethyl 3, 3′-dithiobispropionimidate (DTBP) as a cleavable disμLfide-based polymer to encapsμLate nucleic acids in biological sample preparation[J]. *Sensors and Actuators B: Chemical*, 2019, 288: 225-231.

28. Koo B, Jin C E, Lee T Y, et al. An isothermal, label-free, and rapid one-step RNA amplification/detection assay for diagnosis of respiratory viral infections[J]. *Biosensors and Bioelectronics*, 2017, 90: 187-194.

29. Jang Y O, Jin C E, Choi E H, et al. A homobifunctional imidoester-based microfluidic system for simμLtaneous DNA and protein isolation from solid or liquid biopsy samples[J]. *Lab on a Chip*, 2019, 19(13): 2256-2264.

30. Yoon J, Park M K, Lee T Y, et al. LoMA-B: a simple and versatile lab-on-a-chip system based on single-channel bisμLfite conversion for DNA methylation analysis[J]. *Lab on a Chip*, 2015, 15(17): 3530-3539.

31. Jin, Liguo, et al. "Fast Acting Black Phosphorus Assisted Depression Therapy with Low Toxicity." *Advanced Materials* 32.2 (2020): 1906050.

32. Choi J R, Yong K W, Choi J Y, et al. Black phosphorus and its biomedical applications[J]. *Theranostics*, 2018, 8(4): 1005.

33. Luo M, Fan T, Zhou Y, et al. 2D black phosphorus–based biomedical applications[J]. *Advanced Functional Materials*, 2019, 29(13): 1808306.

34. Chen W, Ouyang J, Yi X, et al. Black phosphorus nanosheets as a neuroprotective

nanomedicine for neurodegenerative disorder therapy[J]. *Advanced materials*, 2018, 30(3): 1703458.

35. Luo M, Fan T, Zhou Y, et al. 2D black phosphorus–based biomedical applications[J]. Advanced Functional Materials, 2019, 29(13): 1808306.

36. Li B, Lai C, Zeng G, et al. Black Phosphorus, A Rising Star 2D Nanomaterial in the Post Graphene Era: Synthesis, Properties, Modifications, and Photocatalysis Applications[J]. Small, 2019, 15(8): 1804565.

6. ABSTRACT IN KOREAN

항생제 남용에 따른 세균 내성은 세계에서 가장 큰 공중보건 문제 중 하나다. 첨단 나노기술이 항생제 생산에 활용되고 있지만 혈액 응결, 독성, 저효능, 저생물상용성 등의 부작용에 대한 대응은 새로운 나노복합재료가 필요하다. 본 연구에서는 동일한 생물학적 기능을 하는 동형 2 기 이미도에스터가 코팅된 산화아연 나노구조체(HINS) 를 합성해 항생제의 효능을 높이고 독성과 응혈 작용을 감소시키는 간단한 방법을 소개했다. 이 복합소재의 항생제 효능은 상업 아연 나노입자의 두배다. 또 동형 2 기 이미도에스터의 아세틸화기 때문에 생체상용성이 뛰어나 표면 전하와 용해도를 증가시키고 Zn2+ 이온과 방어적 활성산소(ROS)를 다량 발생시켜 세균과 진균을 죽이는 데 효과적이다. 체외와 체내 실험에서 정맥내에서 HINS 나노구조체와 이트라코나졸의 시너지 작용으로 진균의 파괴율이 90%를 넘는 것으로 나타났다. 따라서 의학 분야에서는 HINS 나노구조체를 사용해 항생제 남용의 영향을 줄일 수 있다. 또한 BP 는 새로운 2 차원 나노 소재로 의학적 항종양과 생체센서에서 광열과 제약성능이 뛰어나다. BP 의 광열 특성을 이용한 질병 진단 등의 연구를 처음으로 시도해, 보다 편리하고 빠른 진단 기술을 제공한다. 여기서 우리는 BP 에 레이저를 쬐어 대장균을 분해해 DNA 를 분열시킨 뒤 동형 2 기 이미도에스터와 BP 구조체를 이용해서 DNA 를 결합한다. 상품화된 QIAGEN 보다 DNA 의 추출에 더 도움이 됩니다. 또 실시간 PCR 기술을 통해 DNA 추출 효율이 현저히 향상됨을 확인하였다. 병원체 분자 진단에서 BP 구조체의 활용은 미래 진단 발전 방향에 대한 새로운 아이디어를 통한 기반을 마련하는데 큰 도움이 되었다.

키워드: 나노소재, 다이내믹아미드 에스테르, 항균, DNA 추출